

SPATIOSPECTRAL CONCENTRATION ON A SPHERE*

FREDERIK J. SIMONS[†], F. A. DAHLEN[‡], AND MARK A. WIECZOREK[§]

Abstract. We pose and solve the analogue of Slepian's time-frequency concentration problem on the surface of the unit sphere to determine an orthogonal family of strictly bandlimited functions that are optimally concentrated within a closed region of the sphere, or, alternatively, of strictly spacelimited functions that are optimally concentrated within the spherical harmonic domain. Such a basis of simultaneously spatially and spectrally concentrated functions should be a useful data analysis and representation tool in a variety of geophysical and planetary applications, as well as in medical imaging, computer science, cosmology and numerical analysis. The spherical Slepian functions can be found either by solving an algebraic eigenvalue problem in the spectral domain or by solving a Fredholm integral equation in the spatial domain. The associated eigenvalues are a measure of the spatio-spectral concentration. When the concentration region is an axisymmetric polar cap the spatio-spectral projection operator commutes with a Sturm-Liouville operator; this enables the eigenfunctions to be computed extremely accurately and efficiently, even when their area-bandwidth product, or Shannon number, is large. In the asymptotic limit of a small concentration region and a large spherical harmonic bandwidth the spherical concentration problem approaches its planar equivalent, which exhibits self-similarity when the Shannon number is kept invariant.

Key words. bandlimited function, commuting differential operator, concentration problem, eigenvalue problem, multitaper spectral analysis, spherical harmonic

AMS subject classifications. 42B05, 42B35, 45B05, 47B32

1. Introduction. In a classic series of papers published in the 1960's, David Slepian and his colleagues solved a fundamental problem in communications engineering, namely that of optimally concentrating a signal in both the time and frequency domains [32; 33; 53; 54; 56]. The orthogonal family of data windows, or tapers, that arise in this context, and their multi-dimensional extensions [20; 36] have been used as the basis for the multitaper method of spectral analysis [46; 61], and for the analysis and representation of data in a wide range of physical, computational and biomedical disciplines (e.g., geodesy, seismology, optics, information theory, neurology and speech recognition). Time-frequency and time-scale concentration operators have been studied in more general settings and a variety of one- and multi-dimensional geometries by several authors [e.g., 10; 11; 13; 15; 35; 41; 42].

In this paper we consider the simultaneous spatial and spectral concentration of a real-valued function of geographical position on the surface of the unit sphere. The spherical multitapers that we derive here should be useful in a number of geophysical and planetary data analysis applications; this is our primary motivation to undertake the present study. In particular, we note that physical properties, such as the thickness or elastic strength of a planetary lithosphere, can be estimated from the cross-spectral properties of the surface topography and associated gravitational field [63]. Such data are most commonly available as bandlimited spherical harmonic coefficients, measured by artificial satellites or spacecraft. In many if not most applications, planetary curvature prohibits the use of locally flat approximations [65]. Thus, the determination of spatially localized estimates of planetary properties re-

*Received by the editors February 1, 2008.

[†]Department of Geosciences, Princeton University, Princeton NJ 08544, U.S.A. Now at: Department of Earth Sciences, University College, London WC1E 6BT, United Kingdom.

[‡]Department of Geosciences, Princeton University, Princeton NJ 08544, U.S.A.

[§]Département de Géophysique Spatiale et Planétaire, Institut de Physique du Globe de Paris, 94701 St. Maur-des-Fossés, France.

quires spatio-spectral localization methods that go beyond those available in the plane [e.g., 50]. Single spherical windows or tapers have been developed and applied in a number of recent studies [e.g., 16; 17; 29; 52]; however, these are neither optimally concentrated, nor as reliable as an orthogonal family of multitapers in the extraction of robust localized statistical information from bandlimited spherical data [66].

Following an initial and extremely insightful analysis by Grünbaum and his colleagues [19], Slepian's concentration problem on a sphere has, to our knowledge, been revisited quite rarely, by workers interested in geodesy [1], magnetic resonance imaging of the human brain [47] and planetary spectral analysis [66]. Each of these studies treats a special case. In this paper, we pose and solve the spherical spatio-spectral concentration problem in its most general form, discuss a number of numerical implementation methods, and analyze the flat-earth asymptotic limit, in which the spherical concentration problem approaches the corresponding problem on a plane.

2. Slepian concentration problem. We begin with a brief review of the one-dimensional, continuous-continuous, time-frequency concentration problem. The results are well known so we shall just articulate them without providing any derivations; our only objective is to provide a template for the spherical concentration problem, which we consider in the remainder of the paper. We use t and ω to denote time and angular frequency, respectively, and adopt a normalization convention in which a real time-domain signal $f(t)$ and its Fourier transform $F(\omega)$ are related by

$$(2.1) \quad f(t) = \frac{1}{2\pi} \int_{-\infty}^{\infty} F(\omega) e^{i\omega t} d\omega, \quad F(\omega) = \int_{-\infty}^{\infty} f(t) e^{-i\omega t} dt.$$

The specific problem considered by Slepian [56] is that of optimally concentrating a strictly bandlimited signal $g(t)$, with a spectrum $G(\omega)$ that vanishes for frequencies $|\omega| > W$, into a time interval $|t| \leq T$. No such bandlimited signal $g(t)$ can be completely concentrated within a finite interval by virtue of the Heisenberg uncertainty principle [14; 39]; the optimally concentrated signal is considered to be the one with the least energy outside of the interval:

$$(2.2) \quad \lambda = \frac{\int_{-T}^T g^2(t) dt}{\int_{-\infty}^{\infty} g^2(t) dt} = \text{maximum}.$$

Bandlimited signals $g(t)$ satisfying the variational problem (2.2) have spectra $G(\omega)$ that satisfy the frequency-domain convolutional integral eigenvalue equation

$$(2.3) \quad \int_{-W}^W \frac{\sin T(\omega - \omega')}{\pi(\omega - \omega')} G(\omega') d\omega' = \lambda G(\omega), \quad |\omega| \leq W.$$

A closely related problem is that of concentrating the spectrum $H(\omega)$ of a strictly timelimited function $h(t)$, that vanishes for times $|t| > T$, into a spectral interval $|\omega| \leq W$. The appropriate measure of concentration in this case is

$$(2.4) \quad \lambda = \frac{\int_{-W}^W |H(\omega)|^2 d\omega}{\int_{-\infty}^{\infty} |H(\omega)|^2 d\omega} = \text{maximum}.$$

Timelimited signals $h(t)$ whose spectra satisfy the variational problem (2.4) themselves satisfy the time-domain eigenvalue equation

$$(2.5) \quad \int_{-T}^T \frac{\sin W(t-t')}{\pi(t-t')} h(t') dt' = \lambda h(t), \quad |t| \leq T.$$

Both equations (2.3) and (2.5) have the same eigenvalues $1 > \lambda_1 > \lambda_2 > \dots > 0$, with associated time-domain eigentapers $g_1(t), g_2(t), \dots$ and $h_1(t), h_2(t), \dots$ which coincide within the interval $|t| \leq T$, and associated eigenspectra $G_1(\omega), G_2(\omega), \dots$ and $H_1(\omega), H_2(\omega), \dots$ which coincide within the interval $|\omega| \leq W$.

A change of both the independent and dependent variables transforms both (2.3) and (2.5) into the same dimensionless eigenvalue equation:

$$(2.6) \quad \int_{-1}^1 \frac{\sin TW(x-x')}{\pi(x-x')} \psi(x') dx' = \lambda \psi(x), \quad |x| \leq 1.$$

Equation (2.6) shows that the eigenvalues $\lambda_1, \lambda_2, \dots$ and suitably scaled eigenfunctions $\psi_1(x), \psi_2(x), \dots$ depend only upon the time-bandwidth product TW . The sum of the eigenvalues is related to this product by

$$(2.7) \quad N = \sum_{\alpha=1}^{\infty} \lambda_{\alpha} = \frac{2TW}{\pi}.$$

Because of the characteristic step shape of the eigenvalue spectrum [30; 57], this so-called Shannon number [46] is a good estimate of the number of significant eigenvalues, or, roughly speaking, the number of signals $f(t)$ that can be simultaneously well concentrated into a finite time interval $|t| \leq T$ and a finite frequency interval $|\omega| \leq W$.

The integral operator acting upon ψ on the left side of equation (2.6) commutes with a second-order differential operator,

$$(2.8) \quad \mathcal{P} = \frac{d}{dx}(1-x^2)\frac{d}{dx} - T^2W^2x^2,$$

which arises in the separation of the three-dimensional scalar wave equation in prolate spheroidal coordinates [55]. Because of this, it is also possible to find the scaled eigenfunctions $\psi_1(x), \psi_2(x), \dots$ by solving the Sturm-Liouville equation

$$(2.9) \quad \frac{d}{dx}(1-x^2)\frac{d\psi}{dx} + (\chi - T^2W^2x^2)\psi = 0, \quad |x| \leq 1,$$

where $\chi \neq \lambda$ is the associated eigenvalue.

The bandlimited prolate spheroidal eigentapers may be chosen to be orthonormal over the infinite time interval $|t| \leq \infty$ and orthogonal over the finite interval $|t| \leq T$:

$$(2.10) \quad \int_{-\infty}^{\infty} g_{\alpha}g_{\beta} dt = \delta_{\alpha\beta} \quad \text{and} \quad \int_{-T}^T g_{\alpha}g_{\beta} dt = \lambda_{\alpha} \delta_{\alpha\beta}.$$

Almost all of the above results can be extended to the analogous spatio-spectral concentration problem for functions defined on the surface of the unit sphere. As we shall see, this two-dimensional problem is enriched by the arbitrary shape of the region of spatial concentration.

3. Preliminaries. The geometry of the unit sphere $\Omega = \{\hat{\mathbf{r}} : \|\hat{\mathbf{r}}\| = 1\}$ is depicted in Figure 3.1. We denote the colatitude of a point $\hat{\mathbf{r}}$ by $0 \leq \theta \leq \pi$ and the longitude by $0 \leq \phi < 2\pi$, so that $\hat{\mathbf{r}} = (\theta, \phi)$ represents a geographical position on the sphere. The geodesic angular distance between two points $\hat{\mathbf{r}}$ and $\hat{\mathbf{r}}'$ will be denoted by Δ , where

$$(3.1) \quad \cos \Delta = \hat{\mathbf{r}} \cdot \hat{\mathbf{r}}' = \cos \theta \cos \theta' + \sin \theta \sin \theta' \cos(\phi - \phi').$$

We use R to denote a region of Ω of area A , within which we seek to concentrate a bandlimited function of position $\hat{\mathbf{r}}$. The region may consist of a number of unconnected subregions, $R = R_1 \cup R_2 \cup \dots$, and it may have an irregularly shaped boundary, as shown. The region complementary to R will be denoted by $\Omega - R$.

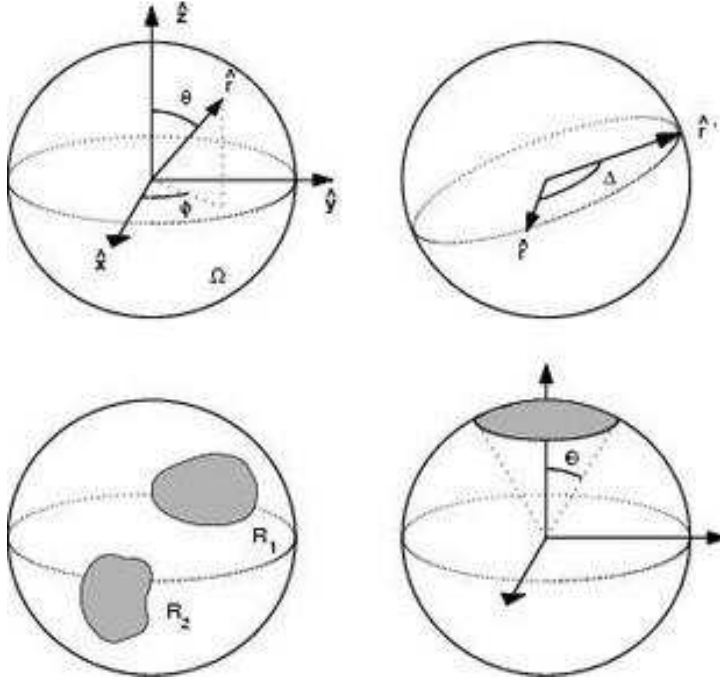


FIG. 3.1. Sketch illustrating the geometry of the spherical concentration problem. Lower right shows an axisymmetric polar cap of colatitudinal radius Θ , treated in Section 5. The area of the region of concentration, $R = R_1 \cup R_2 \cup \dots$, is denoted by A .

3.1. Spherical harmonics. Since we restrict attention to real-valued functions, we use real surface spherical harmonics $Y_{lm}(\hat{\mathbf{r}}) = Y_{lm}(\theta, \phi)$ defined by [9; 12]

$$(3.2) \quad Y_{lm}(\theta, \phi) = \begin{cases} \sqrt{2}X_{l|m|}(\theta) \cos m\phi & \text{if } -l \leq m < 0 \\ X_{l0}(\theta) & \text{if } m = 0 \\ \sqrt{2}X_{lm}(\theta) \sin m\phi & \text{if } 0 < m \leq l, \end{cases}$$

$$(3.3) \quad X_{lm}(\theta) = (-1)^m \left(\frac{2l+1}{4\pi} \right)^{1/2} \left[\frac{(l-m)!}{(l+m)!} \right]^{1/2} P_{lm}(\cos \theta),$$

$$(3.4) \quad P_{lm}(\mu) = \frac{1}{2^l l!} (1 - \mu^2)^{m/2} \left(\frac{d}{d\mu} \right)^{l+m} (\mu^2 - 1)^l.$$

The quantity $0 \leq l \leq \infty$ is known as the angular degree of the spherical harmonic, and $-l \leq m \leq l$ is its angular order. The $l \rightarrow \infty$ asymptotic wavenumber associated with a harmonic of degree l is $\sqrt{l(l+1)} \approx l + 1/2$ [5; 26]. The function $P_{lm}(\mu)$ defined in (3.4) is the associated Legendre function of integer degree l and order m . The spherical harmonics $Y_{lm}(\hat{\mathbf{r}})$ are eigenfunctions of the Laplace-Beltrami operator,

$$(3.5) \quad \nabla^2 = \partial_\theta^2 + \cot \theta \partial_\theta + (\sin \theta)^{-2} \partial_\phi^2,$$

with associated eigenvalues $-l(l+1)$. Our choice of the multiplicative constants in equations (3.2) and (3.3) orthonormalizes the harmonics on the unit sphere:

$$(3.6) \quad \int_{\Omega} Y_{lm} Y_{l'm'} d\Omega = \delta_{ll'} \delta_{mm'}.$$

The corresponding fixed-order orthogonality relations for $X_{lm}(\theta)$ and $P_{lm}(\mu)$ are

$$(3.7a) \quad \int_0^\pi X_{lm} X_{l'm} \sin \theta d\theta = \frac{1}{2\pi} \delta_{ll'},$$

$$(3.7b) \quad \int_{-1}^1 P_{lm} P_{l'm} d\mu = \frac{2}{2l+1} \frac{(l+m)!}{(l-m)!} \delta_{ll'}.$$

The integral of a Legendre polynomial $P_l(\mu) = P_{l0}(\mu)$ over a cap $\cos \Theta \leq \mu \leq 1$ is [6]

$$(3.8) \quad \int_{\cos \Theta}^1 P_l d\mu = \frac{1}{2l+1} [P_{l-1}(\cos \Theta) - P_{l+1}(\cos \Theta)],$$

where $P_{-1}(\mu) = 1$, and the product of Legendre functions at the same argument is

$$(3.9) \quad \begin{aligned} X_{lm}(\theta) X_{l'm}(\theta) &= (-1)^m \sum_{n=|l-l'|}^{l+l'} \sqrt{\frac{(2n+1)(2l+1)(2l'+1)}{4\pi}} \\ &\times \begin{pmatrix} l & n & l' \\ 0 & 0 & 0 \end{pmatrix} \begin{pmatrix} l & n & l' \\ m & 0 & -m \end{pmatrix} X_{n0}(\theta), \end{aligned}$$

where the arrays of indices are Wigner 3- j symbols [12; 39]. Of the numerous three-term recursion relations involving the associated Legendre functions and their derivatives, we shall make use of two in this paper, namely

$$(3.10a) \quad (2l+1)\mu P_{lm} = (l-m+1)P_{l+1,m} + (l+m)P_{l-1,m},$$

$$(3.10b) \quad (1-\mu^2) \frac{dP_{lm}}{d\mu} = (l+1)\mu P_{lm} - (l-m+1)P_{l+1,m}.$$

Finally, there are two relations involving sums of products of Legendre functions evaluated at different arguments that are useful in the discussion that follows. The first is the well-known spherical harmonic addition theorem [12]

$$(3.11) \quad \sum_{m=-l}^l Y_{lm}(\hat{\mathbf{r}}) Y_{lm}(\hat{\mathbf{r}}') = \left(\frac{2l+1}{4\pi} \right) P_l(\hat{\mathbf{r}} \cdot \hat{\mathbf{r}}'),$$

and the second is the Legendre version of the Christoffel-Darboux identity [59; 60]

$$(3.12) \quad \begin{aligned} & (\mu - \mu') \sum_{l=m}^L (2l+1) \left[\frac{(l-m)!}{(l+m)!} \right] P_{lm}(\mu) P_{lm}(\mu') \\ &= \frac{(L-m+1)!}{(L+m)!} [P_{L+1,m}(\mu) P_{Lm}(\mu') - P_{Lm}(\mu) P_{L+1,m}(\mu')]. \end{aligned}$$

An application of L'Hôpital's rule in equation (3.12) covers the case when $\mu = \mu'$.

3.2. Functions on the sphere. Let $f(\hat{\mathbf{r}})$ be a real-valued, square-integrable function on the unit sphere Ω . Any such function can be expanded as a series of spherical harmonics:

$$(3.13) \quad f = \sum_{l=0}^{\infty} \sum_{m=-l}^l f_{lm} Y_{lm}, \quad f_{lm} = \int_{\Omega} f Y_{lm} d\Omega.$$

Equations (3.13) are the spherical analogue of the one-dimensional Fourier transform pair (2.1). The finite character of the unit sphere quantizes the colatitudinal and longitudinal “frequencies” $0 \leq l \leq \infty$ and $-l \leq m \leq l$. We use a sans serif \mathbf{f} to denote the ordered column vector of spherical harmonic coefficients:

$$(3.14) \quad \mathbf{f} = \begin{pmatrix} \vdots \\ f_{lm} \\ \vdots \end{pmatrix}.$$

The norm of a function $f(\hat{\mathbf{r}})$ in the spatial domain will be denoted by

$$(3.15) \quad \|f\|_{\Omega}^2 = \int_{\Omega} f^2 d\Omega,$$

and the norm of its spectral-domain equivalent \mathbf{f} will be denoted by

$$(3.16) \quad \|\mathbf{f}\|_{\infty}^2 = \sum_{l=0}^{\infty} \sum_{m=-l}^l f_{lm}^2.$$

Using this notation, Parseval's relation [46] can be written in the form $\|f\|_{\Omega}^2 = \|\mathbf{f}\|_{\infty}^2$. The power spectral density or variance per spherical harmonic degree l and per unit area of a function $f(\hat{\mathbf{r}})$ is defined by

$$(3.17) \quad \langle f_l^2 \rangle = \frac{1}{2l+1} \sum_{m=-l}^l f_{lm}^2.$$

We use $\delta(\hat{\mathbf{r}}, \hat{\mathbf{r}}')$ for the Dirac delta function on the sphere, with the replication property

$$(3.18) \quad \int_{\Omega} \delta(\hat{\mathbf{r}}, \hat{\mathbf{r}}') f(\hat{\mathbf{r}}') d\Omega' = f(\hat{\mathbf{r}}).$$

We can write $\delta(\hat{\mathbf{r}}, \hat{\mathbf{r}}')$ in any of the alternative forms

$$\delta(\hat{\mathbf{r}}, \hat{\mathbf{r}}') = (\sin \theta)^{-1} \delta(\theta - \theta') \delta(\phi - \phi')$$

$$\begin{aligned}
&= \sum_{l=0}^{\infty} \sum_{m=-l}^l Y_{lm}(\hat{\mathbf{r}}) Y_{lm}(\hat{\mathbf{r}}') \\
(3.19) \quad &= \sum_{l=0}^{\infty} \left(\frac{2l+1}{4\pi} \right) P_l(\hat{\mathbf{r}} \cdot \hat{\mathbf{r}}').
\end{aligned}$$

The degree variance of a delta function is constant; its power spectral density is white:

$$(3.20) \quad \langle \delta_l^2 \rangle = \frac{1}{4\pi} \quad \text{for all } 0 \leq l \leq \infty.$$

3.3. Bandlimited and spacelimited functions. We are interested in two subspaces of the space of all square-integrable functions on the unit sphere Ω . We use

$$(3.21) \quad \mathcal{S}_L = \{g : \langle g_l^2 \rangle = 0 \text{ for } L < l \leq \infty\}$$

to denote the space of all bandlimited functions,

$$(3.22) \quad g = \sum_{l=0}^L \sum_{m=-l}^l g_{lm} Y_{lm},$$

with no power above a maximal spherical harmonic degree L , and we use

$$(3.23) \quad \mathcal{S}_R = \{h : h = 0 \text{ in } \Omega - R\}$$

to denote the space of all spacelimited functions $h(\hat{\mathbf{r}})$ that are strictly contained within a region R . The space \mathcal{S}_R is infinite-dimensional, but the dimension of the space of bandlimited functions is

$$(3.24) \quad \dim \mathcal{S}_L = \sum_{l=0}^L (2l+1) = (L+1)^2,$$

since the ordered column vector of spherical harmonic coefficients

$$(3.25) \quad \mathbf{g} = \begin{pmatrix} g_{00} \\ \vdots \\ g_{LL} \end{pmatrix}$$

associated with a function $g(\hat{\mathbf{r}})$ of the form (3.22) has $(L+1)^2$ entries. Spatial and spectral seminorms analogous to (3.15) and (3.16) are defined as

$$(3.26) \quad \|f\|_R^2 = \int_R f^2 d\Omega, \quad \|\mathbf{f}\|_L^2 = \sum_{l=0}^L \sum_{m=-l}^l f_{lm}^2.$$

Within the space \mathcal{S}_R of spacelimited functions, $\|h\|_R^2$ is a norm, and within the space \mathcal{S}_L of bandlimited functions, $\|\mathbf{g}\|_L^2$ is a norm; more generally, however, both $\|f\|_R^2$ and $\|\mathbf{f}\|_L^2$ are seminorms.

4. Concentration within an arbitrarily shaped region. The uncertainty principle [14; 39] stipulates that no function can be both strictly spacelimited and strictly bandlimited, i.e., no $f(\mathbf{r})$ can lie in both subspaces \mathcal{S}_R and \mathcal{S}_L simultaneously. The objective of this paper is to determine those bandlimited functions $g(\mathbf{r}) \in \mathcal{S}_L$ that are as well contained within a spatial region R as possible, and those spacelimited functions $h(\mathbf{r}) \in \mathcal{S}_R$ whose power spectrum is as well concentrated within the interval $0 \leq l \leq L$ as possible. As in the time-frequency case, these two spatio-spectral concentration problems will be shown to be each other's duals. For brevity, in the discussion that follows, we shall frequently use the abbreviations

$$(4.1) \quad \sum_{l=0}^{\infty} \sum_{m=-l}^l = \sum_{lm}^{\infty} \quad \text{and} \quad \sum_{l=0}^L \sum_{m=-l}^l = \sum_{lm}^L.$$

4.1. Spatial concentration of a bandlimited function. To maximize the spatial concentration of a bandlimited function $g(\mathbf{r}) \in \mathcal{S}_L$ within a region R , we maximize the ratio of the (semi)norms:

$$(4.2) \quad \lambda = \frac{\|g\|_R^2}{\|g\|_{\Omega}^2} = \frac{\int_R g^2 d\Omega}{\int_{\Omega} g^2 d\Omega} = \text{maximum}.$$

The two-dimensional variational problem (4.2) is analogous to the one-dimensional problem (2.2). Here, as there, the quantity $0 < \lambda < 1$ is a measure of the spatial concentration. Upon inserting the representation (3.22) of $g(\mathbf{r})$ into (4.2), and interchanging the order of summation and integration, we can express λ in the form

$$(4.3) \quad \begin{aligned} \lambda &= \frac{\int_R \left(\sum_{lm}^L g_{lm} Y_{lm} \sum_{l'm'}^L g_{l'm'} Y_{l'm'} \right) d\Omega}{\int_{\Omega} \left(\sum_{lm}^L g_{lm} Y_{lm} \sum_{l'm'}^L g_{l'm'} Y_{l'm'} \right) d\Omega} \\ &= \frac{\sum_{lm}^L g_{lm} \sum_{l'm'}^L \left(\int_R Y_{lm} Y_{l'm'} d\Omega \right) g_{l'm'}}{\sum_{lm}^L g_{lm} \sum_{l'm'}^L \left(\int_{\Omega} Y_{lm} Y_{l'm'} d\Omega \right) g_{l'm'}} \\ &= \frac{\sum_{lm}^L g_{lm} \sum_{l'm'}^L D_{lm,l'm'} g_{l'm'}}{\sum_{lm}^L g_{lm}^2}, \end{aligned}$$

where in the final step we have used the orthonormality relation (3.6), and defined the quadruply indexed quantity

$$(4.4) \quad D_{lm,l'm'} = \int_R Y_{lm} Y_{l'm'} d\Omega.$$

Upon introducing the $(L+1)^2 \times (L+1)^2$ matrix

$$(4.5) \quad \mathbf{D} = \begin{pmatrix} D_{00,00} & \cdots & D_{00,LL} \\ \vdots & & \vdots \\ D_{LL,00} & \cdots & D_{LL,LL} \end{pmatrix},$$

with elements $D_{lm,l'm'}$, where $0 \leq l \leq L$ and $-l \leq m \leq l$, we can rewrite equation (4.2) as a classical matrix variational problem [22] in the space \mathcal{S}_L :

$$(4.6) \quad \lambda = \frac{\mathbf{g}^T \mathbf{D} \mathbf{g}}{\mathbf{g}^T \mathbf{g}} = \text{maximum}.$$

Column vectors \mathbf{g} that render the Rayleigh quotient λ in equation (4.6) stationary are solutions of the $(L+1)^2 \times (L+1)^2$ algebraic eigenvalue problem

$$(4.7) \quad \mathbf{D} \mathbf{g} = \lambda \mathbf{g}.$$

Equation (4.7) is the discrete spherical analogue of the one-dimension spectral-domain equation (2.3). The matrix \mathbf{D} is real, symmetric and positive definite,

$$(4.8) \quad \mathbf{D}^T = \mathbf{D} \quad \text{and} \quad \mathbf{g}^T \mathbf{D} \mathbf{g} > 0 \quad \text{for all } \mathbf{g} \neq \mathbf{0},$$

so the $(L+1)^2$ eigenvalues λ and associated eigenvectors \mathbf{g} are always real [22]. We order the eigenvalues $\lambda_1, \lambda_2, \dots, \lambda_{(L+1)^2}$ and eigenvectors $\mathbf{g}_1, \mathbf{g}_2, \dots, \mathbf{g}_{(L+1)^2}$ so that

$$(4.9) \quad 1 > \lambda_1 \geq \lambda_2 \geq \dots \geq \lambda_{(L+1)^2} > 0.$$

Each spectral-domain eigenvector \mathbf{g}_α , $\alpha = 1, 2, \dots, (L+1)^2$ gives rise to an associated bandlimited spatial eigenfunction $g_\alpha(\hat{\mathbf{r}})$, defined by equation (3.22). The first inequality in (4.9) is strict because no bandlimited function can be completely confined within a region R , and the last inequality is strict because of the positive-definite character of the matrix \mathbf{D} .

The symmetry $\mathbf{D}^T = \mathbf{D}$ also guarantees that the eigenvectors $\mathbf{g}_1, \mathbf{g}_2, \dots, \mathbf{g}_{(L+1)^2}$ are mutually orthogonal [22]. We choose them to be orthonormal:

$$(4.10) \quad \mathbf{g}_\alpha^T \mathbf{g}_\beta = \delta_{\alpha\beta} \quad \text{and} \quad \mathbf{g}_\alpha^T \mathbf{D} \mathbf{g}_\beta = \lambda_\alpha \delta_{\alpha\beta}.$$

The associated spatial eigenfunctions $g_1(\hat{\mathbf{r}}), g_2(\hat{\mathbf{r}}), \dots, g_{(L+1)^2}(\hat{\mathbf{r}})$ are in that case both orthonormal over the whole sphere Ω and orthogonal over the region R :

$$(4.11) \quad \int_{\Omega} g_\alpha g_\beta d\Omega = \delta_{\alpha\beta} \quad \text{and} \quad \int_R g_\alpha g_\beta d\Omega = \lambda_\alpha \delta_{\alpha\beta}.$$

The two spatial-domain relations in equation (4.11) are equivalent to the corresponding matrix spectral relations (4.10), and they are analogous to the one-dimensional orthogonality relations (2.10). The eigenfunction $g_1(\hat{\mathbf{r}})$ associated with the largest eigenvalue λ_1 is the member of the space \mathcal{S}_L of bandlimited functions that is most spatially concentrated within the the region R , the eigenfunction $g_2(\hat{\mathbf{r}})$ is the next best concentrated function in \mathcal{S}_L orthogonal to $g_1(\hat{\mathbf{r}})$ over both Ω and R , and so on.

Written out in full using index notation, the matrix eigenvalue equation (4.7) is

$$(4.12) \quad \sum_{l'm'}^L D_{lm,l'm'} g_{l'm'} = \lambda g_{lm}.$$

Upon multiplying equation (4.12) by $Y_{lm}(\hat{\mathbf{r}})$ and summing over all $0 \leq l \leq L$ and $-l \leq m \leq l$, the right side yields $\lambda g(\hat{\mathbf{r}})$, and the left can be manipulated as follows:

$$\begin{aligned}
 \sum_{lm}^L \left(\sum_{l'm'}^L D_{lm,l'm'} g_{l'm'} \right) Y_{lm}(\hat{\mathbf{r}}) &= \sum_{lm}^L \sum_{l'm'}^L \left(\int_R Y_{lm}(\hat{\mathbf{r}}') Y_{l'm'}(\hat{\mathbf{r}}') d\Omega' \right) g_{l'm'} Y_{lm}(\hat{\mathbf{r}}) \\
 &= \int_R \left(\sum_{lm}^L Y_{lm}(\hat{\mathbf{r}}) Y_{lm}(\hat{\mathbf{r}}') \right) \left(\sum_{l'm'}^L g_{l'm'} Y_{l'm'}(\hat{\mathbf{r}}') \right) d\Omega' \\
 (4.13) \qquad &= \int_R D(\hat{\mathbf{r}}, \hat{\mathbf{r}}') g(\hat{\mathbf{r}}') d\Omega',
 \end{aligned}$$

where in the final step we have defined the bandlimited Dirac delta function

$$(4.14) \qquad D(\hat{\mathbf{r}}, \hat{\mathbf{r}}') = \sum_{l=0}^L \sum_{m=-l}^l Y_{lm}(\hat{\mathbf{r}}) Y_{lm}(\hat{\mathbf{r}}') = \sum_{l=0}^L \left(\frac{2l+1}{4\pi} \right) P_l(\hat{\mathbf{r}} \cdot \hat{\mathbf{r}}').$$

The above derivation demonstrates that the spectral-domain matrix eigenvalue equation (4.7) is equivalent to the spatial-domain integral eigenvalue equation

$$(4.15) \qquad \int_R D(\hat{\mathbf{r}}, \hat{\mathbf{r}}') g(\hat{\mathbf{r}}') d\Omega' = \lambda g(\hat{\mathbf{r}}), \quad \hat{\mathbf{r}} \in \Omega.$$

Equation (4.15) is a homogeneous Fredholm integral equation of the second kind, with a symmetric, separable kernel [28; 62]. Upon inserting the representations (3.22) and (4.14) into equation (4.15), we recover the matrix equation (4.7), so that the spectral-domain eigenvalue problem for \mathbf{g} and the spatial-domain eigenvalue problem for a bandlimited $g(\hat{\mathbf{r}}) \in \mathcal{S}_L$ are completely equivalent.

In summary, we can find an orthogonal family of bandlimited eigenfunctions that are optimally concentrated within a region R on the unit sphere Ω either by solving the $(L+1)^2 \times (L+1)^2$ matrix eigenvalue problem (4.7) for the spectral-domain eigenvectors $\mathbf{g}_1, \mathbf{g}_2, \dots, \mathbf{g}_{(L+1)^2}$, or by solving the Fredholm integral equation (4.15) for the associated spatial-domain eigenfunctions $g_1, g_2, \dots, g_{(L+1)^2}$. Either method determines the optimally concentrated eigenfunctions at all points $\hat{\mathbf{r}} \in \Omega$, i.e., both in the region R , where they are concentrated, and in the complementary region $\Omega - R$, where they exhibit inevitable leakage.

4.2. Spectral concentration of a spacelimited function. Instead of seeking to concentrate a bandlimited function $g(\hat{\mathbf{r}}) \in \mathcal{S}_L$ within a spatial region R , we may seek to concentrate a spacelimited function $h(\hat{\mathbf{r}}) \in \mathcal{S}_R$ within a spectral interval $0 \leq l \leq L$. A suitable measure of concentration is then the spectral norm ratio, analogous to the one-dimensional ratio (2.4):

$$(4.16) \qquad \lambda = \frac{\|\mathbf{h}\|_L^2}{\|\mathbf{h}\|_\infty^2} = \frac{\sum_{l=0}^L \sum_{m=-l}^l h_{lm}^2}{\sum_{l=0}^\infty \sum_{m=-l}^l h_{lm}^2} = \text{maximum}.$$

Upon inserting the representation of the spherical harmonic expansion coefficients,

$$(4.17) \qquad h_{lm} = \int_R h Y_{lm} d\Omega,$$

and interchanging the order of summation and integration, we can rewrite the ratio (4.16) in the form

$$\begin{aligned}
 \lambda &= \frac{\sum_{lm} \int_R h(\hat{\mathbf{r}}) Y_{lm}(\hat{\mathbf{r}}) d\Omega \int_R h(\hat{\mathbf{r}}') Y_{lm}(\hat{\mathbf{r}}') d\Omega'}{\sum_{lm} \int_R h(\hat{\mathbf{r}}) Y_{lm}(\hat{\mathbf{r}}) d\Omega \int_R h(\hat{\mathbf{r}}') Y_{lm}(\hat{\mathbf{r}}') d\Omega'} \\
 &= \frac{\int_R \int_R h(\hat{\mathbf{r}}) \left(\sum_{lm}^L Y_{lm}(\hat{\mathbf{r}}) Y_{lm}(\hat{\mathbf{r}}') \right) h(\hat{\mathbf{r}}') d\Omega' d\Omega}{\int_R \int_R h(\hat{\mathbf{r}}) \left(\sum_{lm}^\infty Y_{lm}(\hat{\mathbf{r}}) Y_{lm}(\hat{\mathbf{r}}') \right) h(\hat{\mathbf{r}}') d\Omega' d\Omega} \\
 (4.18) \quad &= \frac{\int_R \int_R h(\hat{\mathbf{r}}) D(\hat{\mathbf{r}}, \hat{\mathbf{r}}') h(\hat{\mathbf{r}}') d\Omega d\Omega'}{\int_R h^2(\hat{\mathbf{r}}) d\Omega},
 \end{aligned}$$

where in the final step we have made use of replication property (3.18) of the delta function (3.19) and the definition (4.14) of the kernel $D(\hat{\mathbf{r}}, \hat{\mathbf{r}}')$. Functions $h(\hat{\mathbf{r}}) \in \mathcal{S}_R$ that render the Rayleigh quotient (4.18) stationary are solutions of the Fredholm integral eigenvalue equation

$$(4.19) \quad \int_R D(\hat{\mathbf{r}}, \hat{\mathbf{r}}') h(\hat{\mathbf{r}}') d\Omega' = \lambda h(\hat{\mathbf{r}}), \quad \hat{\mathbf{r}} \in R.$$

Equation (4.19) is the spherical analogue of the one-dimensional time-domain eigenvalue equation (2.5). In fact, this equation for $h(\hat{\mathbf{r}}) \in \mathcal{S}_R$ is identical to equation (4.15) for $g(\hat{\mathbf{r}}) \in \mathcal{S}_L$. The only difference is that equation (4.15) is applicable on the entire sphere Ω , whereas the domain of equation (4.19) is limited to the region R , within which $h(\hat{\mathbf{r}}) \neq 0$. Evidently, the eigenfunctions $h(\hat{\mathbf{r}})$ that maximize the spectral norm ratio (4.16) are identical, within the region R , to the eigenfunctions $g(\hat{\mathbf{r}})$ that maximize the spatial norm ratio (4.2):

$$(4.20) \quad h(\hat{\mathbf{r}}) = \begin{cases} g(\hat{\mathbf{r}}) & \text{if } \hat{\mathbf{r}} \in R \\ 0 & \text{otherwise.} \end{cases}$$

Every one of the $(L+1)^2$ bandlimited eigenfunctions $g_\alpha \in \mathcal{S}_L$ gives rise to a space-limited eigenfunction $h_\alpha \in \mathcal{S}_R$, defined by the restriction (4.20). The associated eigenvalues λ_α are a measure of both the spatial concentration of the bandlimited eigenfunctions within the region R and the spectral concentration of the spacelimited eigenfunctions within the interval $0 \leq l \leq L$. The fractional spatial energy $1 - \lambda_\alpha$ leaked by an eigenfunction $g_\alpha(\hat{\mathbf{r}})$ to the region $\Omega - R$ is identical to the fractional spectral energy leaked by $h_\alpha(\hat{\mathbf{r}})$ into the higher degrees $L < l \leq \infty$. If we had started with the variational prescription (4.16) rather than (4.2), we could have obtained the integral equation (4.15) governing a bandlimited function $g(\hat{\mathbf{r}}) \in \mathcal{S}_L$ by simply extending the domain of solution of equation (4.19) to the whole sphere Ω .

The spacelimited eigenfunctions defined by equation (4.20) are orthogonal but not orthonormal over the whole sphere Ω and over the region R :

$$(4.21) \quad \int_\Omega h_\alpha h_\beta d\Omega = \int_R h_\alpha h_\beta d\Omega = \lambda_\alpha \delta_{\alpha\beta}.$$

The spherical harmonic coefficients h_{lm} , with $0 \leq l \leq \infty$ and $-l \leq m \leq l$, are given in terms of those of g_{lm} , with $0 \leq l \leq L$ and $-l \leq m \leq l$, by

$$(4.22) \quad h_{lm} = \sum_{l'=0}^L \sum_{m'=-l'}^{l'} D_{lm,l'm'} g_{l'm'},$$

which reduces to $h_{lm} = \lambda g_{lm}$ for $0 \leq l \leq L$. In addition to the $(L+1)^2$ eigenfunctions with associated non-zero eigenvalues $\lambda_1, \lambda_2, \dots, \lambda_{(L+1)^2}$, equation (4.19) has an infinite-dimensional null space of eigenfunctions with associated eigenvalue $\lambda = 0$. Every function $h(\mathbf{r})$ that vanishes in $\Omega - R$ and has no energy whatsoever in the interval $0 \leq l \leq L$ is a member of this null space.

4.3. Significant and insignificant eigenvalues. The sum of the eigenvalues of the matrix \mathbf{D} defined in equation (4.5) is

$$(4.23) \quad N = \sum_{\alpha=1}^{(L+1)^2} \lambda_{\alpha} = \text{tr } \mathbf{D} = \sum_{l=0}^L \sum_{m=-l}^l D_{lm,lm}.$$

Upon substituting for the diagonal matrix elements $D_{lm,lm}$ from equation (4.4) and making use of the spherical harmonic addition theorem (3.11), this simplifies to

$$(4.24) \quad \begin{aligned} N &= \sum_{l=0}^L \sum_{m=-l}^l \int_R Y_{lm} Y_{lm} d\Omega \\ &= \sum_{l=0}^L \int_R \left(\sum_{m=-l}^l Y_{lm} Y_{lm} \right) d\Omega \\ &= \sum_{l=0}^L \left(\frac{2l+1}{4\pi} \right) \int_R P_l(1) d\Omega \\ &= (L+1)^2 \frac{A}{4\pi}, \end{aligned}$$

where in the final step we have used the identity $P_l(1) = 1$ to express the result in terms of the surface area, $A = \int_R d\Omega$, of the region of concentration R .

We can alternatively obtain the result (4.23) by starting with the spatial eigenvalue equation (4.15). The kernel $D(\mathbf{r}, \mathbf{r}')$ can be expressed in terms of the spatial eigenfunctions $g_1, g_2, \dots, g_{(L+1)^2}$, which constitute a basis for \mathcal{S}_L , in the form

$$(4.25) \quad D(\mathbf{r}, \mathbf{r}') = \sum_{\alpha=1}^{(L+1)^2} g_{\alpha}(\mathbf{r}) g_{\alpha}(\mathbf{r}').$$

The representation (4.25) is the spherical analogue of Mercer's theorem [28; 62]. Algebraically, we can regard the relation (4.25) as having been obtained from the original representation (4.14) by an orthogonal transformation from one basis, Y_{lm} , $0 \leq l \leq L$ and $-l \leq m \leq l$, to another, g_{α} , $\alpha = 1, 2, \dots, (L+1)^2$. Setting $\mathbf{r}' = \mathbf{r}$ in equation (4.25), and integrating over the region R , we obtain

$$(4.26) \quad \int_R D(\mathbf{r}, \mathbf{r}) d\Omega = \sum_{\alpha=1}^{(L+1)^2} \int_R g_{\alpha}^2(\mathbf{r}) d\Omega = \sum_{\alpha=1}^{(L+1)^2} \lambda_{\alpha}.$$

Alternatively, setting $\hat{\mathbf{r}}' = \hat{\mathbf{r}}$ in equation (4.14) and integrating over R yields

$$(4.27) \quad \int_R D(\hat{\mathbf{r}}, \hat{\mathbf{r}}) d\Omega = \sum_{l=0}^L \left(\frac{2l+1}{4\pi} \right) \int_R P_l(1) d\Omega = (L+1)^2 \frac{A}{4\pi}.$$

Comparing equations (4.23)–(4.24) and (4.26)–(4.27), we see that we can write the sum of the eigenvalues (4.23) in any of the equivalent ways

$$(4.28) \quad N = \sum_{\alpha=1}^{(L+1)^2} \lambda_{\alpha} = \text{tr } \mathbf{D} = \int_R D(\hat{\mathbf{r}}, \hat{\mathbf{r}}) d\Omega = (L+1)^2 \frac{A}{4\pi}.$$

The quantity N is the spherical analogue of the Shannon number (2.7) in Slepian's one-dimensional concentration problem. Eigenfunctions $g_{\alpha}(\hat{\mathbf{r}})$ that are well concentrated within the region R will have associated eigenvalues λ_{α} that are near unity, whereas those that are poorly concentrated will have associated eigenvalues λ_{α} that are near zero. If, as in the one-dimensional problem, the spectrum of eigenvalues $\lambda_1, \lambda_2, \dots, \lambda_{(L+1)^2}$ has a narrow transition band from values near unity to values near zero, then the total number of significant ($\lambda_{\alpha} \approx 1$) eigenvalues will be well approximated by the (rounded) sum (4.23). For this reason, we expect N to be a good estimate of the number of significant eigenvalues. Roughly speaking, the spherical Shannon number (4.28) is the dimension of the space of two-dimensional functions $f(\hat{\mathbf{r}})$ that are both approximately limited in the spectral domain to spherical harmonic degrees $0 \leq l \leq L$ and approximately limited in the spatial domain to an arbitrarily shaped region R of area A [30; 31].

Rather than seeking a bandlimited function $g(\hat{\mathbf{r}}) \in \mathcal{S}_L$ that is optimally concentrated within a spatial region R , we could have decided to seek one that is optimally excluded from R , i.e., one that is optimally concentrated within the complementary region $\Omega - R$. In that case we would have sought to minimize rather than maximize the Rayleigh quotient (4.2). In fact, all that we have found are the bandlimited functions $g(\hat{\mathbf{r}}) \in \mathcal{S}_L$ that render the eigenvalue λ stationary, so we have actually solved the containment problem (4.2) and the exclusion problem simultaneously. The optimally concentrated eigenfunctions and the optimally excluded eigenfunctions are identical, but with the ordering indices reversed, i.e., the bandlimited function that is most excluded from R and most concentrated within $\Omega - R$ is $g_{(L+1)^2}(\hat{\mathbf{r}})$, with the smallest associated eigenvalue $\lambda_{(L+1)^2}$. Whenever the area A of the region R is a small fraction of the area of the sphere, $A \ll 4\pi$, there will be many more well excluded eigenfunctions with insignificant ($\lambda_{\alpha} \approx 0$) eigenvalues, than well concentrated eigenfunctions with significant ($\lambda_{\alpha} \approx 1$) eigenvalues, i.e., $N \ll (L+1)^2$.

The sum of the squares of the $(L+1)^2$ bandlimited eigenfunctions $g_{\alpha}(\hat{\mathbf{r}})$ is a constant, independent of position $\hat{\mathbf{r}}$ on the sphere Ω . This is another consequence of Mercer's theorem (4.25) and the definition (4.14):

$$(4.29) \quad \sum_{\alpha=1}^{(L+1)^2} g_{\alpha}^2(\hat{\mathbf{r}}) = D(\hat{\mathbf{r}}, \hat{\mathbf{r}}) = \frac{(L+1)^2}{4\pi} = \frac{N}{A}.$$

If the first N eigenfunctions g_1, g_2, \dots, g_N have eigenvalues near unity and lie mostly within R , and the remainder $g_{N+1}, g_{N+2}, \dots, g_{(L+1)^2}$ have eigenvalues near zero and lie mostly in $\Omega - R$, then we expect the eigenvalue-weighted sum of squares to be

$$(4.30) \quad \sum_{\alpha=1}^{(L+1)^2} \lambda_{\alpha} g_{\alpha}^2(\hat{\mathbf{r}}) \approx \sum_{\alpha=1}^N \lambda_{\alpha} g_{\alpha}^2(\hat{\mathbf{r}}) \approx \begin{cases} N/A & \text{if } \hat{\mathbf{r}} \in R \\ 0 & \text{otherwise.} \end{cases}$$

The terms with $N + 1 \leq \alpha \leq (L + 1)^2$ should be negligible, so it is immaterial whether they are included in the sum (4.30) or not. Taken together, the first N orthogonal eigenfunctions $g_\alpha, \alpha = 1, 2, \dots, N$, with significant eigenvalues $\lambda_\alpha \approx 1$, provide an essentially uniform coverage of the region R . This is really the essence of the spatio-spectral concentration problem; the number of degrees of freedom is reduced from $\dim \mathcal{S}_L = (L + 1)^2$ to the Shannon number $N = (L + 1)^2 A / (4\pi)$.

4.4. Abstract operator formulation. We conclude this section on the concentration problem for an arbitrarily shaped region by reiterating the above results using an abstract operator notation. We use \mathcal{H} to denote the operator that acts upon square-integrable functions $f(\hat{\mathbf{r}})$ in the spatial domain to produce the associated infinite-dimensional column vectors \mathbf{f} of spherical harmonic coefficients f_{lm} in the spectral domain, and we use \mathcal{H}^{-1} to denote its inverse, so that

$$(4.31) \quad \mathcal{H}f = \mathbf{f} \quad \text{and} \quad \mathcal{H}^{-1}\mathbf{f} = f.$$

We also introduce two projection operators, \mathcal{R} and \mathcal{L} , which project onto the space \mathcal{S}_R of spacelimited functions and the space \mathcal{S}_L of bandlimited functions, respectively. The first of these acts to spatially restrict functions $f(\hat{\mathbf{r}})$ in the spatial domain,

$$(4.32) \quad \mathcal{R}f(\hat{\mathbf{r}}) = \begin{cases} f(\hat{\mathbf{r}}) & \text{if } \hat{\mathbf{r}} \in R \\ 0 & \text{otherwise,} \end{cases}$$

whereas the second acts to bandlimit column vectors in the spectral domain,

$$(4.33) \quad \mathcal{L}\mathbf{f} = \mathcal{L} \begin{pmatrix} f_{00} \\ \vdots \\ f_{\infty\infty} \end{pmatrix} = \begin{pmatrix} f_{00} \\ \vdots \\ f_{LL} \end{pmatrix}.$$

Finally, we introduce a notation for the standard inner product in both domains:

$$(4.34) \quad \langle f, f' \rangle_\Omega = \int_\Omega f f' d\Omega \quad \text{and} \quad \langle \mathbf{f}, \mathbf{f}' \rangle_\infty = \mathbf{f}^\top \mathbf{f}'.$$

Parseval's relation can be written using this notation in the form $\langle f, f' \rangle_\Omega = \langle \mathbf{f}, \mathbf{f}' \rangle_\infty$. The spatial and spectral norms introduced in equations (3.15) and (3.16) are given by $\|f\|_\Omega^2 = \langle f, f \rangle_\Omega$ and $\|\mathbf{f}\|_\infty^2 = \langle \mathbf{f}, \mathbf{f} \rangle_\infty$.

The spatial-concentration variational problem (4.2) and the spectral-concentration variational problem (4.16) can be written using this operator notation in the form

$$(4.35a) \quad \lambda = \frac{\langle \mathcal{R}\mathcal{H}^{-1}\mathcal{L}\mathbf{f}, \mathcal{R}\mathcal{H}^{-1}\mathcal{L}\mathbf{f} \rangle_\Omega}{\langle \mathcal{H}^{-1}\mathcal{L}\mathbf{f}, \mathcal{H}^{-1}\mathcal{L}\mathbf{f} \rangle_\Omega} = \text{maximum},$$

$$(4.35b) \quad \lambda = \frac{\langle \mathcal{L}\mathcal{H}\mathcal{R}f, \mathcal{L}\mathcal{H}\mathcal{R}f \rangle_\infty}{\langle \mathcal{H}\mathcal{R}f, \mathcal{H}\mathcal{R}f \rangle_\infty} = \text{maximum}.$$

The associated spectral and spatial-domain eigenvalue equations are

$$(4.36a) \quad (\mathcal{L}\mathcal{H}\mathcal{R}\mathcal{H}^{-1}\mathcal{L})(\mathcal{L}\mathbf{f}) = \lambda(\mathcal{L}\mathbf{f}),$$

$$(4.36b) \quad (\mathcal{R}\mathcal{H}^{-1}\mathcal{L}\mathcal{H}\mathcal{R})(\mathcal{R}f) = \lambda(\mathcal{R}f),$$

where we have made use of the facts that \mathcal{H} and \mathcal{H}^{-1} are each others' transposes, that both \mathcal{R} and \mathcal{L} are their own transposes, and that $\mathcal{R}^2 = \mathcal{R}$ and $\mathcal{L}^2 = \mathcal{L}$. Equations (4.36) are the operator equivalents of the algebraic eigenvalue equation (4.7) and

the integral eigenvalue equation (4.19). Any solution of equation (4.36a) is a band-limited column vector of the form $\mathbf{g} = \mathcal{L}\mathbf{f}$, whereas any solution of equation (4.36b) is a spacelimited function of the form $h = \mathcal{R}f$. Both the spectral-domain operator $\mathcal{L}\mathcal{H}\mathcal{R}\mathcal{H}^{-1}\mathcal{L}$ and the spatial-domain operator $\mathcal{R}\mathcal{H}^{-1}\mathcal{L}\mathcal{H}\mathcal{R}$ are symmetric by inspection. Application of the operator product $\mathcal{H}^{-1}\mathcal{L}\mathcal{H}$ acts to bandlimit an arbitrary function f , an operation referred to as spherical or uniform-resolution filtering, or as triangular truncation, in numerical analysis [4; 25; 44; 59].

5. Concentration within an axisymmetric polar cap. We turn our attention next to the special but important case in which the region of concentration is a circularly symmetric cap of colatitudinal radius Θ , centered on the north pole, as illustrated in the lower right of Figure 3.1:

$$(5.1) \quad R = \{\theta : 0 \leq \theta \leq \Theta\}.$$

In practical applications, the eigenfunctions that are optimally concentrated within such a polar cap can be rotated to an arbitrarily positioned circular cap on the unit sphere using standard spherical harmonic rotation formulae [3; 9; 12; 37].

5.1. Decomposition of the spectral-domain eigenvalue problem. The matrix elements (4.4) reduce in the case (5.1) to

$$(5.2) \quad D_{lm,l'm'} = 2\pi \delta_{mm'} \int_0^\Theta X_{lm} X_{l'm'} \sin \theta d\theta.$$

The Kronecker delta $\delta_{mm'}$ renders the matrix \mathbf{D} in equation (4.5) block-diagonal:

$$(5.3) \quad \mathbf{D} = \begin{pmatrix} \mathbf{D}_0 & & & & \\ & \mathbf{D}_{\pm 1} & & & \\ & & \mathbf{D}_{\pm 1} & & \\ & & & \ddots & \\ & & & & \mathbf{D}_{\pm L} \\ & & & & & \mathbf{D}_{\pm L} \end{pmatrix},$$

where every $(L - m + 1) \times (L - m + 1)$ submatrix $\mathbf{D}_{\pm m} \neq \mathbf{D}_0$ occurs twice as a result of the doublet degeneracy associated with $\pm m$. Rather than solving the full $(L+1)^2 \times (L+1)^2$ eigenvalue equation (4.7), we may solve a series of smaller eigenvalue equations, $\mathbf{D}_{\pm m} \mathbf{g}_{\pm m} = \lambda_{\pm m} \mathbf{g}_{\pm m}$, one for each order $\pm m$.

We shall henceforth drop the identifying subscript and rewrite the fixed-order, spectral-domain algebraic eigenvalue problem $\mathbf{D}_{\pm m} \mathbf{g}_{\pm m} = \lambda_{\pm m} \mathbf{g}_{\pm m}$ as, simply,

$$(5.4) \quad \mathbf{D} \mathbf{g} = \lambda \mathbf{g}.$$

The $(L - m + 1) \times (L - m + 1)$ matrix \mathbf{D} and the $(L - m + 1)$ -dimensional column vector $\mathbf{g} \in \mathcal{S}_L$ are of the form

$$(5.5) \quad \mathbf{D} = \begin{pmatrix} D_{mm} & \cdots & D_{mL} \\ \vdots & & \vdots \\ D_{Lm} & \cdots & D_{LL} \end{pmatrix} \quad \text{and} \quad \mathbf{g} = \begin{pmatrix} g_m \\ \vdots \\ g_L \end{pmatrix},$$

where, for a particular order m ,

$$(5.6) \quad D_{ll'} = 2\pi \int_0^\Theta X_{lm} X_{l'm} \sin \theta d\theta.$$

The integral in equation (5.6) can be evaluated with the aid of equations (3.8)–(3.9):

$$(5.7) \quad D_{ll'} = (-1)^m \frac{\sqrt{(2l+1)(2l'+1)}}{2} \sum_{n=|l-l'|}^{l+l'} \begin{pmatrix} l & n & l' \\ 0 & 0 & 0 \end{pmatrix} \begin{pmatrix} l & n & l' \\ m & 0 & -m \end{pmatrix} \times [P_{n-1}(\cos \Theta) - P_{n+1}(\cos \Theta)].$$

We rank order the distinct $L - m + 1$ eigenvalues $\lambda_1, \lambda_2, \dots, \lambda_{L-m+1}$ obtained by solving the fixed-order eigenvalue problem (5.4) so that

$$(5.8) \quad 1 > \lambda_1 > \lambda_2 > \dots > \lambda_{L-m+1} > 0,$$

and orthonormalize the $(L - m + 1)$ -dimensional eigenvectors $\mathbf{g}_1, \mathbf{g}_2, \dots, \mathbf{g}_{L-m+1}$ as

$$(5.9) \quad \mathbf{g}_\alpha^\top \mathbf{g}_\beta = \delta_{\alpha\beta} \quad \text{and} \quad \mathbf{g}_\alpha^\top \mathbf{D} \mathbf{g}_\beta = \lambda_\alpha \delta_{\alpha\beta}.$$

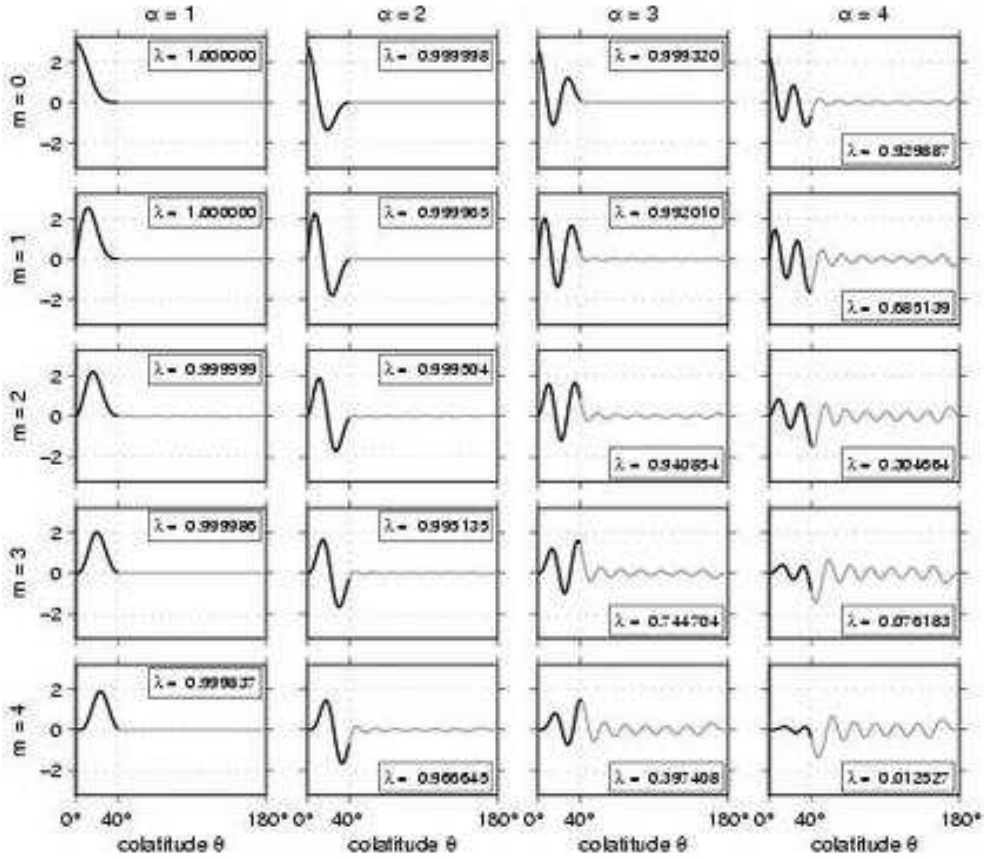


FIG. 5.1. Colatitudinal dependence of the first four spatial-domain eigenfunctions $g_1(\theta), g_2(\theta), g_3(\theta), g_4(\theta)$ of fixed order $m = 0$ (top) to $m = 4$ (bottom). The radius of the polar cap is $\Theta = 40^\circ$, and the maximal spherical harmonic degree is $L = 18$. Black curves show the concentration within the cap $0 \leq \theta \leq 40^\circ$; grey curves highlight the leakage into the rest of the sphere, $40^\circ < \theta \leq 180^\circ$. The eigenvalues $\lambda_1, \lambda_2, \lambda_3, \lambda_4$ expressing the goodness of the spatial concentration are indicated. The corresponding leakage in the spectral domain is illustrated in Figure 5.2.

The associated bandlimited eigenfunctions $g_1(\theta), g_2(\theta), \dots, g_{L-m+1}(\theta)$, defined by

$$(5.10) \quad g(\theta) = \sum_{l=m}^L g_l X_{lm}(\theta),$$

then satisfy the colatitudinal orthogonality relations

$$(5.11) \quad 2\pi \int_0^\pi g_\alpha g_\beta \sin \theta d\theta = \delta_{\alpha\beta} \quad \text{and} \quad 2\pi \int_0^\Theta g_\alpha g_\beta \sin \theta d\theta = \lambda_\alpha \delta_{\alpha\beta}.$$

The optimally concentrated spatial eigenfunctions $g(\hat{\mathbf{r}})$ for a given m are expressed in terms of the fixed-order colatitudinal eigenfunctions (5.10) by

$$(5.12) \quad g(\theta, \phi) = \begin{cases} \sqrt{2} g(\theta) \cos m\phi & \text{if } -L \leq m < 0 \\ g(\theta) & \text{if } m = 0 \\ \sqrt{2} g(\theta) \sin m\phi & \text{if } 0 < m \leq L. \end{cases}$$

The four most optimally concentrated eigenfunctions $g_1(\theta), g_2(\theta), g_3(\theta), g_4(\theta)$, for orders $0 \leq m \leq 4$ are plotted in Figure 5.1. The radius of the polar cap in this example is $\Theta = 40^\circ$, and the maximal spherical harmonic degree is $L = 18$. The first zonal ($m = 0$) eigenfunction, $g_1(\theta)$, has no nodes within the cap $0^\circ \leq \Theta \leq 40^\circ$; the second, $g_2(\theta)$, has one node, and so on. The non-zonal ($m > 0$) eigenfunctions all vanish at the north pole, $\Theta = 0^\circ$. The first four zonal eigenfunctions, the first three $m = 1$ and $m = 2$ eigenfunctions, and the first two $m = 3$ and $m = 4$ eigenfunctions are all very well concentrated ($\lambda > 0.9$), whereas the fourth $m = 3$ and $m = 4$ eigenfunctions exhibit significant leakage ($\lambda < 0.1$). The numerical methods used to compute the results shown here and in ensuing figures are summarized in Appendix A.

5.2. Decomposition of the spatial-domain eigenvalue problem. The integral eigenvalue problem (4.15) in the spatial domain likewise decomposes into a series of fixed-order, one-dimensional Fredholm eigenvalue equations,

$$(5.13) \quad \int_0^\Theta D(\theta, \theta') g(\theta') \sin \theta' d\theta' = \lambda g(\theta), \quad 0 \leq \theta \leq \pi,$$

each with an m -dependent, separable, symmetric kernel,

$$(5.14) \quad D(\theta, \theta') = 2\pi \sum_{l=m}^L X_{lm}(\theta) X_{lm}(\theta').$$

The results (5.13) and (5.14) can either be obtained by multiplying the index form $D_{ll'} g_{l'} = \lambda g_l$ of equation (5.4) by $X_{lm}(\theta)$ and summing over $m \leq l \leq L$, or by substituting the representation (5.10)–(5.12) into equation (4.15), and using the orthogonality of the longitudinal functions $\dots, \sqrt{2} \cos m\phi, \dots, 1, \dots, \sqrt{2} \sin m\phi, \dots$ over the interval $0 \leq \phi < 2\pi$. The $(L-m+1) \times (L-m+1)$ matrix eigenvalue problem (5.4) can in turn be derived starting from the separable Fredholm equation (5.13), so that the fixed-order spectral and spatial eigenvalue problems are completely equivalent. The fixed-order, spacelimited eigenfunctions

$$(5.15) \quad h(\theta) = \begin{cases} g(\theta) & \text{if } 0 \leq \theta \leq \Theta \\ 0 & \text{otherwise} \end{cases}$$

satisfy an equation identical to (5.13), but only within the polar cap itself:

$$(5.16) \quad \int_0^\Theta D(\theta, \theta') h(\theta') \sin \theta' d\theta' = \lambda h(\theta), \quad 0 \leq \theta \leq \Theta.$$

The eigenvalue λ is a measure of both the spatial concentration of $g(\theta) \in \mathcal{S}_L$ within $0 \leq \theta \leq \Theta$ and the spectral concentration of $h(\theta) \in \mathcal{S}_R$ within $0 \leq l \leq L$. The substitution $\mu = \cos \theta$ converts equations (5.13) and (5.16) into

$$(5.17a) \quad \int_{\cos \Theta}^1 D(\mu, \mu') g(\mu') d\mu' = \lambda g(\mu), \quad -1 \leq \mu \leq 1,$$

$$(5.17b) \quad \int_{\cos \Theta}^1 D(\mu, \mu') h(\mu') d\mu' = \lambda h(\mu), \quad \cos \Theta \leq \mu \leq 1.$$

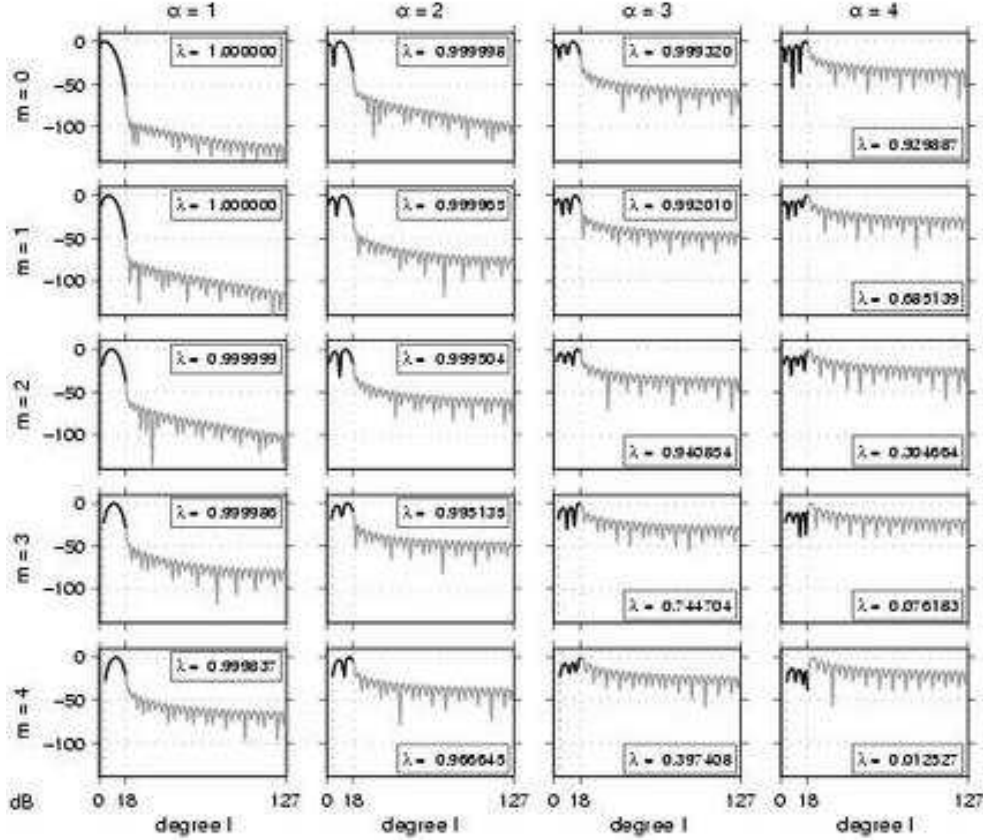


FIG. 5.2. Squared coefficients h_l^2 of the first four spacelimited eigenfunctions $h_1(\theta)$, $h_2(\theta)$, $h_3(\theta)$, $h_4(\theta)$ of fixed order $m = 0$ (top) to $m = 4$ (bottom). The radius of the polar cap is $\Theta = 40^\circ$, and the maximal spherical harmonic degree is $L = 18$. Black curves show the power within the interval of concentration $0 \leq l \leq 18$; grey curves show the leaked power within $19 \leq l \leq 127$. Values of h_l^2 are in dB, normalized to zero at the individual maxima. The eigenvalues $\lambda_1, \lambda_2, \lambda_3, \lambda_4$ specifying the goodness of the spectral concentration are indicated. The corresponding bandlimited, spatial-domain eigenfunctions are shown in Figure 5.1.

The kernel $D(\mu, \mu')$ can be simplified using the Christoffel-Darboux identity (3.12):

$$(5.18) \quad D(\mu, \mu') = \frac{(L-m+1)!}{2(L+m)!} \left[\frac{P_{L+1,m}(\mu)P_{Lm}(\mu') - P_{Lm}(\mu)P_{L+1,m}(\mu')}{\mu - \mu'} \right],$$

where L'Hôpital's rule covers the case $\mu = \mu'$. The squared spherical harmonic coefficients h_l^2 of the four best concentrated spacelimited eigenfunctions $h_1(\theta)$, $h_2(\theta)$, $h_3(\theta)$, $h_4(\theta)$ for $0 \leq m \leq 4$ are plotted versus l in Figure 5.2. The cap radius $\Theta = 40^\circ$, bandwidth $L = 18$, and layout are the same as in Figure 5.1. The maximal contribution to the α th zonal ($m = 0$) eigenfunction comes from the harmonic degree satisfying $\sqrt{l(l+1)} \approx \pi/(\alpha\Theta)$; physically, this corresponds to fitting an integral number of asymptotic wavelengths $2\pi/\sqrt{l(l+1)}$ within the cap of diameter 2Θ .

5.3. Significant fixed-order eigenvalues. The number of significant eigenvalues, or partial Shannon number, for each of the fixed-order eigenvalue problems (5.4), (5.13), (5.16) or (5.17) can be computed using any of the equivalent formulae

$$(5.19) \quad N_m = \sum_{\alpha=1}^{L-m+1} \lambda_\alpha = \sum_{l=m}^L D_{ll} = \int_0^\Theta D(\theta, \theta) d\theta = \int_{\cos \Theta}^1 D(\mu, \mu) d\mu.$$

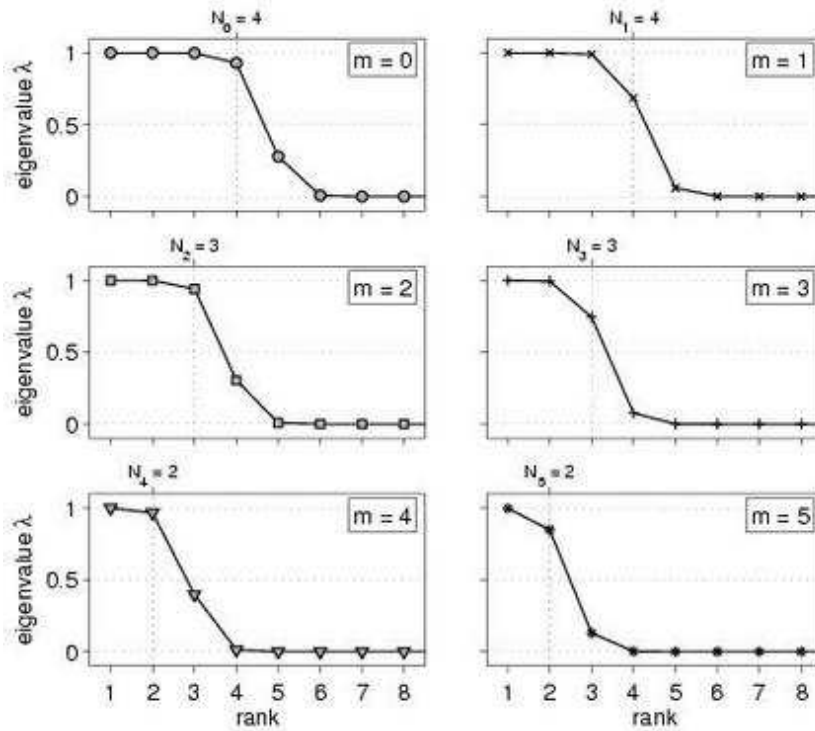


FIG. 5.3. Fixed-order eigenvalue spectra for an axisymmetric polar cap of radius $\Theta = 40^\circ$. The maximal spherical harmonic degree is $L = 18$. A different symbol is used to plot λ_α versus rank α for each order $0 \leq m \leq 5$. The total number of fixed-order eigenvalues is $L - m + 1$; only the largest eight (λ_1 through λ_8) are shown. Vertical gridlines and top labels specify the partial Shannon numbers N_m , rounded to the nearest integer.

We can write the final relation in equation (5.19) using equation (5.18) in the form

$$(5.20) \quad N_m = \frac{(L-m+1)!}{2(L+m)!} \int_{\cos \Theta}^1 [P'_{L+1,m} P_{Lm} - P'_{Lm} P_{L+1,m}] d\mu,$$

where the prime denotes differentiation with respect to μ . Figure 5.3 shows the fixed-order eigenvalue spectra for $0 \leq m \leq 5$. The cap radius is $\Theta = 40^\circ$ and the maximal spherical harmonic degree is $L = 18$, as in Figures 5.1 and 5.2. The partial Shannon numbers N_m , computed by rounding equation (5.19) to the nearest integer, are shown. As in the case of the classical Slepian problem [30; 46; 57] the spectra have a characteristic step shape, showing significant ($\lambda \approx 1$) and insignificant ($\lambda \approx 0$) eigenvalues separated by a narrow transition band. The partial Shannon number (5.19) provides a good estimate of the number of well concentrated eigenfunctions; the first N_m eigenfunctions all have a concentration factor exceeding $\lambda = 0.5$.

Once the $L+1$ sequences of fixed-order eigenvalues (5.8) have been found, they can be resorted in accordance with the mixed-order ranking (4.9). The total number

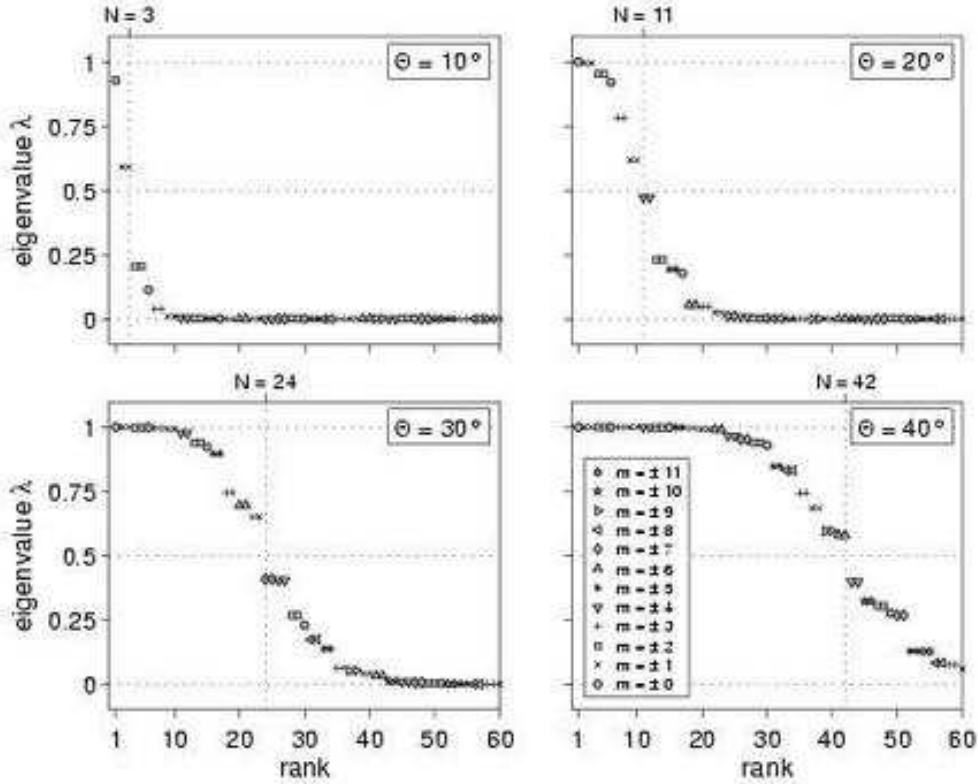


FIG. 5.4. Reordered eigenvalue spectra (λ_α versus rank α) for axisymmetric polar caps of $\Theta = 10^\circ, 20^\circ, 30^\circ, 40^\circ$ and a common maximal spherical harmonic degree $L = 18$. The total number of eigenvalues is $(L+1)^2 = 361$; only λ_1 through λ_{60} are shown. Different symbols are used to plot the various orders $-11 \leq m \leq 11$; the first six symbols are the same as those used in Figure 5.3. Vertical gridlines and top labels specify the rounded Shannon numbers.

of significant eigenvalues is

$$(5.21) \quad N = N_0 + 2 \sum_{m=1}^L N_m,$$

where the factor of two accounts for the $\pm m$ degeneracy. In Figure 5.4 we show the reordered, mixed- m eigenvalue spectra for four different polar caps, with colatitudinal radii $\Theta = 10^\circ, 20^\circ, 30^\circ, 40^\circ$; the maximal spherical harmonic degree is $L = 18$. The rounded Shannon numbers $N = 3, 11, 24, 42$, lie in the middle of the steep, transitional part of the spectra, roughly separating the reasonably well concentrated eigensolutions ($\lambda > 0.5$) from the more poorly concentrated ones ($\lambda < 0.5$) in all four cases.

We illustrate the pointwise sums of squares $\sum_{\alpha} g_{\alpha}^2(\theta, \phi)$ and $\sum_{\alpha} \lambda_{\alpha} g_{\alpha}^2(\theta, \phi)$ in Figure 5.5, for polar caps of radii $\Theta = 10^\circ, 20^\circ, 30^\circ, 40^\circ$ and a bandwidth $L = 18$. The full unweighted sum of $(L+1)^2$ terms (dashed) is equal to $N/A = (L+1)^2/(4\pi)$ over the entire sphere $0^\circ \leq \theta \leq 180^\circ$, in accordance with equation (4.29). The eigenvalue-weighted sums are, in contrast, concentrated within the polar cap $0 \leq \theta \leq \Theta$; solid

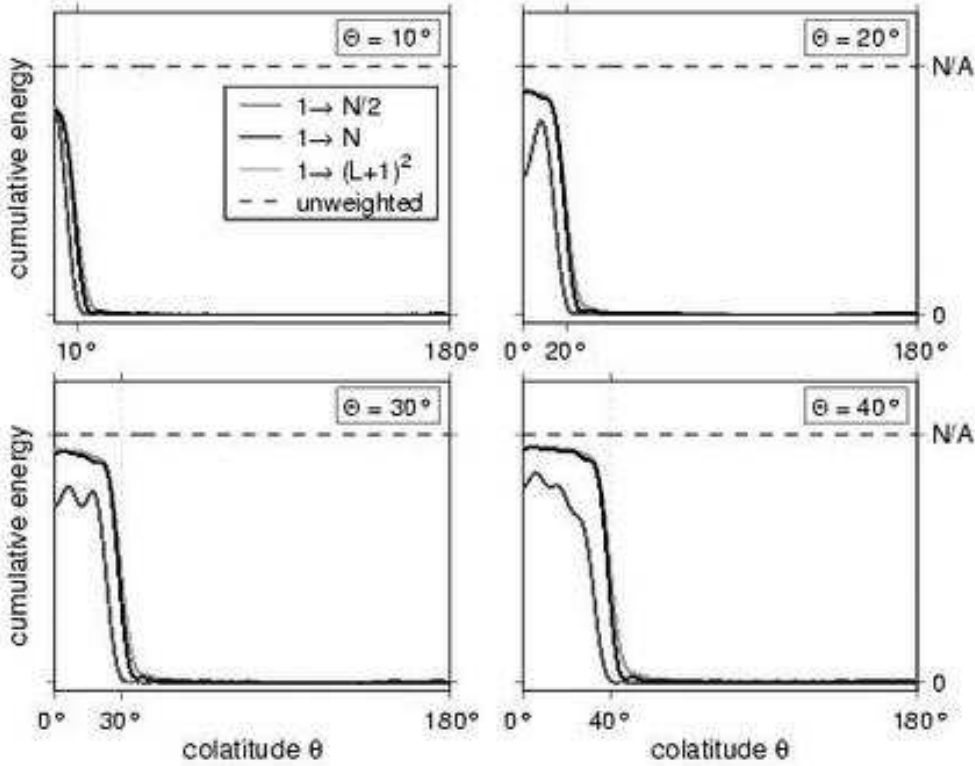


FIG. 5.5. Cumulative energy of the eigenfunctions concentrated within circularly symmetric polar caps of colatitudinal radii $\Theta = 10^\circ, 20^\circ, 30^\circ, 40^\circ$. The maximal spherical harmonic degree is $L = 18$; the Shannon numbers are $N = 3, 11, 24, 42$. The sums of squares $g_1^2(\theta, \phi) + g_2^2(\theta, \phi) + \dots$ and $\lambda_1 g_1^2(\theta, \phi) + \lambda_2 g_2^2(\theta, \phi) + \dots$, are plotted versus colatitude θ along a fixed arbitrary meridian ϕ . Dashed lines show the full unweighted sums of $(L+1)^2$ terms, which converge to the constant value N/A over the entire sphere $0 \leq \theta \leq \pi$. Solid lines show the eigenvalue-weighted partial sums of $N/2$ and N terms, and the full sum of $(L+1)^2$ terms, which are concentrated within the polar cap $0 \leq \theta \leq \Theta$.

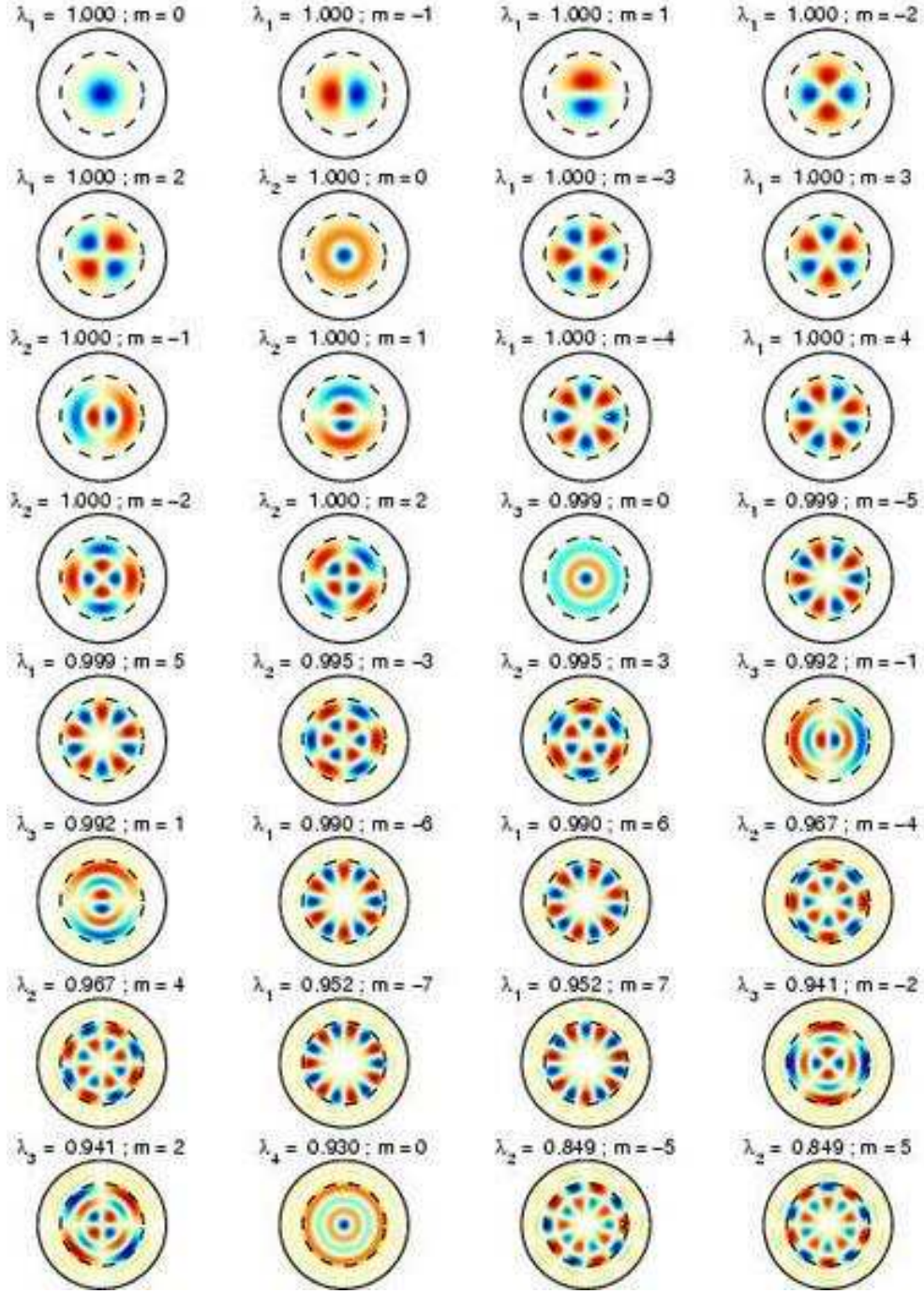


FIG. 5.6. Bandlimited eigenfunctions $g(\theta, \phi)$ that are optimally concentrated within a circular cap of radius $\Theta = 40^\circ$. Dashed circle denotes the cap boundary. The maximal spherical harmonic degree is $L = 18$, and the Shannon number is $N = 42$. Subscripts on the eigenvalues λ_α specify the fixed-order rank. The eigenvalues have been resorted into a mixed-order ranking, with the best concentrated eigenfunction plotted on the top left and the 32nd best on the lower right. Regions in which the absolute value is less than one hundredth of the maximal absolute value on the sphere are rendered in white; blue is positive, and red is negative.

lines of different shades of grey distinguish the sums carried up to the first $N/2$, N , or all $(L+1)^2$ possible terms. Our expectation in equation (4.30) is seen to be well realized. The uniformity of coverage over the region of concentration achieved using only the first N eigentapers is a key result, responsible for the success of the multitaper method of spectral estimation [64]. The utilization of a single, non-oscillatory data taper generally discards information near the boundary; however, this information is recovered by application of the other orthogonal tapers. The energy of the first N tapered data sets is proportional to the original energy of the data within the region of concentration, enabling spatially uniform extraction of statistical information while minimizing spectral leakage [66]. **Mark's change here.**

Finally, Figure 5.6 shows a polar plot of the 32 eigenfunctions $g(\theta, \phi)$, defined by equations (5.12), that are optimally concentrated within a polar cap of radius $\Theta = 40^\circ$. The maximal spherical harmonic degree is $L = 18$ and the Shannon number is $N = 42$, as in Figures 5.1–5.3. The eigenvalue ranking is mixed-order, as in Figure 5.4, and all degenerate $\sqrt{2} \cos m\phi$, $\sqrt{2} \sin m\phi$ doublets are shown. The concentration factors $1 < \lambda < 0.849$ and orders $-5 \leq m \leq 5$ of each eigenfunction are indicated. Blue and red colors represent positive and negative values, respectively; however, all signs could be reversed without violating the quadratic concentration criteria (4.2) and (4.16).

5.4. Commuting differential operator. The analysis of the one-dimensional time-frequency concentration problem was advanced considerably by Slepian's serendipitous discovery of the commuting prolate spheroidal differential operator (2.8). Remarkably, there is also a differential operator, discovered by Grünbaum *et al.* [19], that commutes with the integral operator on the left side of equations (5.16) and (5.17b) [see also 18]. This second-order differential operator is given explicitly by

$$(5.22) \quad \mathcal{G} = (\cos \Theta - \cos \theta) \nabla^2 + \sin \theta \frac{d}{d\theta} - L(L+2) \cos \theta,$$

where

$$(5.23) \quad \nabla^2 = \frac{d^2}{d\theta^2} + \cot \theta \frac{d}{d\theta} - m^2 (\sin \theta)^{-2}$$

is the fixed-order Laplace-Beltrami operator (3.5). Rewritten in terms of $\mu = \cos \theta$, the Grünbaum operator (5.22) is

$$(5.24) \quad \mathcal{G} = \frac{d}{d\mu} \left[(\cos \Theta - \mu)(1 - \mu^2) \frac{d}{d\mu} \right] - L(L+2)\mu - \frac{m^2(\cos \Theta - \mu)}{1 - \mu^2}.$$

Since commuting operators have the same eigenfunctions, we can find the spacelimited, fixed-order eigenfunctions $h(\theta)$ or $h(\mu)$ by solving the differential eigenvalue equation $\mathcal{G}h = \chi h$, where $\chi \neq \lambda$ is the associated Grünbaum eigenvalue.

To confirm that \mathcal{G} in equation (5.24) is the desired commuting differential operator, we are required to show that

$$(5.25) \quad \int_{\cos \Theta}^1 \mathcal{G}_\mu D(\mu, \mu') h(\mu') d\mu' = \int_{\cos \Theta}^1 D(\mu, \mu') \mathcal{G}_{\mu'} h(\mu') d\mu',$$

for an arbitrary spacelimited function $h(\mu)$. There are two steps in the argument given by Grünbaum *et al.* [19]. The first is to show that the right side of equation (5.25) can be rewritten as

$$(5.26) \quad \int_{\cos \Theta}^1 D(\mu, \mu') \mathcal{G}_{\mu'} h(\mu') d\mu' = \int_{\cos \Theta}^1 \mathcal{G}_{\mu'} D(\mu, \mu') h(\mu') d\mu',$$

and the second is to show that

$$(5.27) \quad \mathcal{G}_\mu D(\mu, \mu') = \mathcal{G}_{\mu'} D(\mu, \mu').$$

The first result (5.26) is a straightforward exercise in integration by parts; for any two functions $\zeta(\mu)$ and $\eta(\mu)$, it may be easily shown that

$$(5.28) \quad \int_{\cos \Theta}^1 \zeta(\mathcal{G}\eta) d\mu = - \int_{\cos \Theta}^1 \left[(\cos \Theta - \mu)(1 - \mu^2) \zeta' \eta' + L(L+2)\mu \zeta \eta + m^2(\cos \Theta - \mu)(1 - \mu^2)^{-1} \zeta \eta \right] d\mu = \int_{\cos \Theta}^1 (\mathcal{G}\zeta) \eta d\mu,$$

where we have used a prime to denote $d/d\mu$. Although it is not needed for the proof of equation (5.25), we note for future reference that the result (5.28) is also valid if the integrations are carried out over the full interval $-1 \leq \mu \leq 1$. To verify the second result (5.27) we make use of the relation $\nabla^2 P_{lm} = -l(l+1)P_{lm}$ to write

$$(5.29) \quad \begin{aligned} (\mathcal{G}_\mu - \mathcal{G}_{\mu'}) D(\mu, \mu') = & \\ & + \frac{1}{2} \sum_{l=m}^L [l(l+1) - L(L+2)] (2l+1) \left[\frac{(l-m)!}{(l+m)!} \right] P_{lm}(\mu) P_{lm}(\mu') \\ & - \frac{1}{2} (1 - \mu^2) \sum_{l=m}^L (2l+1) \left[\frac{(l-m)!}{(l+m)!} \right] \frac{d}{d\mu} P_{lm}(\mu) P_{lm}(\mu') \\ & + \frac{1}{2} (1 - \mu'^2) \sum_{l=m}^L (2l+1) \left[\frac{(l-m)!}{(l+m)!} \right] P_{lm}(\mu) \frac{d}{d\mu'} P_{lm}(\mu'). \end{aligned}$$

An application of the Legendre derivative identity (3.10b) transforms (5.29) into

$$(5.30) \quad \begin{aligned} (\mathcal{G}_\mu - \mathcal{G}_{\mu'}) D(\mu, \mu') = & \\ & + \frac{1}{2} (\mu - \mu') \sum_{l=m}^L [l^2 - (L+1)^2] (2l+1) \left[\frac{(l-m)!}{(l+m)!} \right] P_{lm}(\mu) P_{lm}(\mu') \\ & - \frac{1}{2} (\mu - \mu') \sum_{l=m}^L (2l+1) \left[\frac{(l-m+1)!}{(l+m)!} \right] \\ & \times [P_{l+1,m}(\mu) P_{lm}(\mu') - P_{lm}(\mu) P_{l+1,m}(\mu')], \end{aligned}$$

and the Christoffel-Darboux identity (3.12) transforms equation (5.30) into

$$(5.31) \quad \begin{aligned} (\mathcal{G}_\mu - \mathcal{G}_{\mu'}) D(\mu, \mu') = & \\ & + \frac{1}{2} (\mu - \mu') \sum_{l=m}^L [l^2 - (L+1)^2] (2l+1) \left[\frac{(l-m)!}{(l+m)!} \right] P_{lm}(\mu) P_{lm}(\mu') \\ & - \frac{1}{2} (\mu - \mu') \sum_{l=m}^L (2l+1) \sum_{n=m}^l (2n+1) \left[\frac{(n-m)!}{(n+m)!} \right] P_{nm}(\mu) P_{nm}(\mu'). \end{aligned}$$

Interchanging the order of summation in the last line of equation (5.31) we obtain

$$\begin{aligned}
(\mathcal{G}_\mu - \mathcal{G}_{\mu'})D(\mu, \mu') = & \\
& + \frac{1}{2}(\mu - \mu') \sum_{l=m}^L [l^2 - (L+1)^2] (2l+1) \left[\frac{(l-m)!}{(l+m)!} \right] P_{lm}(\mu) P_{lm}(\mu') \\
(5.32) \quad & - \frac{1}{2}(\mu - \mu') \sum_{n=m}^L (2n+1) \left[\frac{(n-m)!}{(n+m)!} \right] P_{nm}(\mu) P_{nm}(\mu') \sum_{l=n}^L (2l+1).
\end{aligned}$$

The final sum over n is equal to $(L+1)^2 - n^2$, so that the two terms in equation (5.32) cancel, $(\mathcal{G}_\mu - \mathcal{G}_{\mu'})D(\mu, \mu') = 0$, and the commutation relation (5.25) is confirmed.

5.5. Grünbaum's equation. The above argument shows that we can compute the fixed-order, spacelimited, colatitudinal eigenfunctions $h_1(\theta), h_2(\theta), \dots, h_{L-m+1}(\theta)$ either by solving the integral equation (5.13) or by solving the differential equation

$$(5.33) \quad (\cos \Theta - \cos \theta) \nabla^2 h + \sin \theta \frac{dh}{d\theta} - L(L+2) \cos \theta h = \chi h, \quad 0 \leq \theta \leq \Theta.$$

The equivalent equation in terms of $\mu = \cos \theta$ is in standard Sturm-Liouville form [7]:

$$(5.34) \quad (ph')' - qh + \chi \rho h = 0, \quad \cos \Theta \leq \mu \leq 1,$$

where the prime denotes differentiation with respect to μ , and where

$$(5.35a) \quad p(\mu) = (\cos \Theta - \mu)(1 - \mu^2),$$

$$(5.35b) \quad q(\mu) = m^2(1 - \mu^2)^{-1}(\mu - \cos \Theta) - L(L+2)\mu,$$

$$(5.35c) \quad \rho(\mu) = 1.$$

Equation (5.34) must be solved subject to the requirement that $h(\mu)$ remain finite at the endpoints $\mu = \cos \Theta$ and $\mu = 1$. The associated variational problem is [7]

$$(5.36) \quad \chi = \frac{\int_{\cos \Theta}^1 (ph'^2 + qh^2) d\mu}{\int_{\cos \Theta}^1 \rho h^2 d\mu} = \text{minimum}.$$

All of the familiar Sturm-Liouville theorems apply. In particular, we know that equation (5.34) has a simple spectrum, with an infinite number of distinct eigenvalues $\chi_1 < \chi_2 < \dots$, having an accumulation point at infinity. The rank orderings of the eigenvalues χ_1, χ_2, \dots and the spatio-spectral concentration factors $\lambda_1, \lambda_2, \dots, \lambda_{L-m+1}$ are reversed, so that the eigenfunction $h_1(\theta)$ associated with the numerically smallest eigenvalue χ_1 , which has no nodes in the polar cap $0 \leq \theta \leq \Theta$, is the most concentrated fixed-order eigenfunction; $h_2(\theta)$, which has exactly one node, is the next best concentrated, and so on. Only the first $L-m+1$ eigenfunctions $h_1(\theta), h_2(\theta), \dots, h_{L-m+1}(\theta)$ with non-zero eigenvalues $\lambda_1, \lambda_2, \dots, \lambda_{L-m+1}$ are of interest in most applications. The remaining eigenfunctions $h_{L-m+2}(\theta), h_{L-m+3}(\theta), \dots$ are in the null space of the integral equation (5.16).

5.6. Commuting tridiagonal matrix. As in the case of (5.13) and (5.16), we are free to extend the domain of equation (5.33) to the entire domain $0 \leq \theta \leq \pi$; in that case, the unknown function must be bandlimited rather than spacelimited:

$$(5.37) \quad (\cos \Theta - \cos \theta) \nabla^2 g + \sin \theta \frac{dg}{d\theta} - L(L+2) \cos \theta g = \chi g, \quad 0 \leq \theta \leq \pi.$$

Upon substituting the harmonic representation (5.10) of $g(\theta)$ into equation (5.37), multiplying both sides by $2\pi \sin \theta X_{l'm}(\theta)$, integrating over $0 \leq \theta \leq \pi$, and invoking the orthogonality relation (3.7b), we obtain the algebraic eigenvalue equation

$$(5.38) \quad \mathbf{G}\mathbf{g} = \chi \mathbf{g},$$

where

$$(5.39) \quad \mathbf{G} = \begin{pmatrix} G_{mm} & \cdots & G_{mL} \\ \vdots & & \vdots \\ G_{Lm} & \cdots & G_{LL} \end{pmatrix}$$

is the $(L-m+1) \times (L-m+1)$ matrix with elements

$$(5.40) \quad G_{ll'} = 2\pi \int_0^\pi X_{lm}(\mathcal{G}X_{l'm}) \sin \theta d\theta.$$

Equation (5.38) is the spectral-domain version of the differential eigenvalue equation (5.37) just as equation (5.4) is the spectral-domain equivalent of the integral eigenvalue equation (5.13).

As we have noted, the symmetry relation (5.28) is valid even if the interval of integration is extended to $0 \leq \theta \leq \pi$, as in equation (5.40). This shows that the Grünbaum matrix \mathbf{G} is symmetric:

$$(5.41) \quad \mathbf{G} = \mathbf{G}^\top.$$

In addition, the matrices \mathbf{D} and \mathbf{G} commute with each other,

$$(5.42) \quad \mathbf{D}\mathbf{G} = \mathbf{G}\mathbf{D},$$

so they have identical eigenvectors. The index version of (5.42) is

$$(5.43) \quad \sum_{n=m}^L D_{ln} G_{nl'} = 2\pi \int_0^\Theta X_{lm}(\mathcal{G}X_{l'm}) \sin \theta d\theta = \sum_{n=m}^L G_{ln} D_{nl'}.$$

The interior expression involving both the operator \mathcal{G} and integration over the region of concentration $0 \leq \theta \leq \Theta$ is the ll' or $l'l$ element of the symmetric matrix product $\mathbf{D}\mathbf{G} = (\mathbf{D}\mathbf{G})^\top$. Verification of the intermediate steps requires the use of the orthogonality relation (3.7b), the operator identity (5.27), and both the symmetry relation (5.28) and its extension to the interval $0 \leq \theta \leq \pi$.

There are a number of ways to evaluate the matrix elements (5.40), perhaps the most straightforward of which is to make use of the relation $\nabla^2 X_{lm} = -l(l+1)X_{lm}$ and the Legendre identities (3.10). In fact, the Grünbaum matrix \mathbf{G} is tridiagonal:

$$(5.44a) \quad G_{ll} = -l(l+1) \cos \Theta,$$

$$(5.44b) \quad G_{l+1,l} = G_{l,l+1} = [l(l+2) - L(L+2)] \sqrt{\frac{(l+1)^2 - m^2}{(2l+1)(2l+3)}},$$

$$(5.44c) \quad G_{ll'} = 0 \quad \text{otherwise,}$$

which is in agreement with the corresponding result given by Grünbaum *et al.* [19].

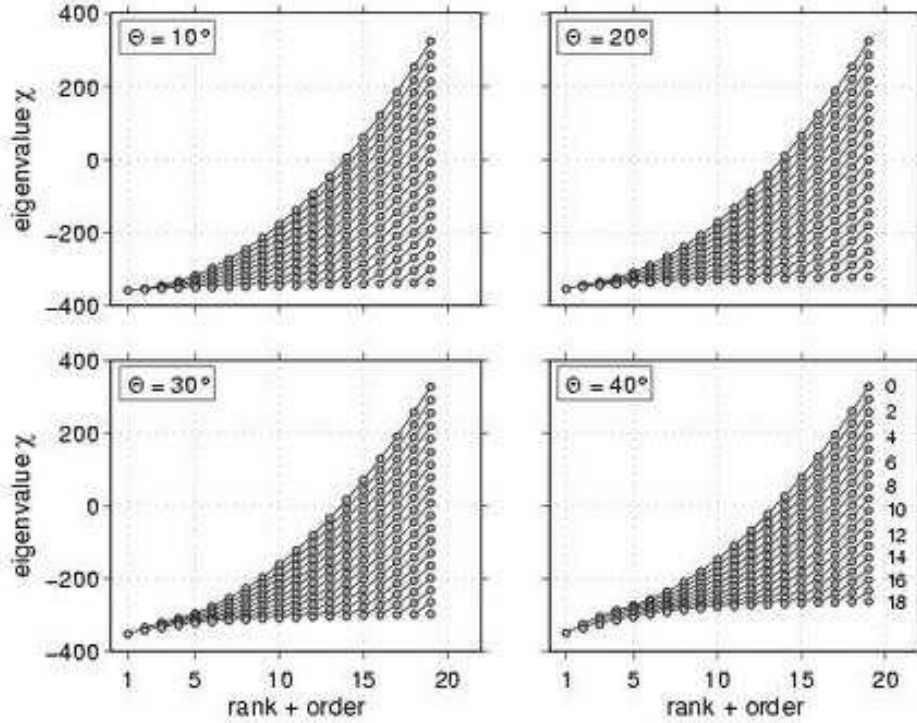


FIG. 5.7. Rank-ordered Grünbaum eigenvalues for polar caps of different colatitudinal radii, $\Theta = 10^\circ, 20^\circ, 30^\circ, 40^\circ$, and a common maximal spherical harmonic degree $L = 18$. Separate sequences of eigenvalues $\chi_1, \chi_2, \dots, \chi_{L-m+1}$ for each angular order $0 \leq m \leq L$ are connected by lines, with each sequence offset horizontally by its order m for clarity.

The solution of equation (5.38) offers a particularly attractive means of computing the eigenvectors $\mathbf{g} \in \mathcal{S}_L$ and thus the optimally concentrated polar cap eigenfunctions $g(\theta) \in \mathcal{S}_L$, because it only requires the numerical diagonalization of a tridiagonal matrix \mathbf{G} with analytically prescribed elements (5.44), and a spectrum of eigenvalues χ that is guaranteed to be simple. To illustrate this, we show the Grünbaum eigenvalue spectra for axisymmetric polar caps of radii $\Theta = 10^\circ, 20^\circ, 30^\circ, 40^\circ$ and a maximal spherical harmonic degree $L = 18$ in Figure 5.7. The ranked eigenvalues for every order $0 \leq m \leq L$ are connected by lines, each sequence offset by its order to facilitate inspection. Thus, $L + 1$ eigenvalues $\chi_1, \chi_2, \dots, \chi_{L+1}$ are plotted for $m = 0$, whereas a single eigenvalue χ_1 is plotted for $m = L$. The roughly equant spacing and absence of a numerically troublesome tail of near-zero values, as in Figures 5.3-5.4, is evident.

Diagonalization of the Grünbaum matrix \mathbf{G} enables the stable computation of optimally concentrated spherical Slepian functions that are bandlimited to very high angular degrees. To illustrate this, we show in Figure 5.8 the first two zonal ($m = 0$) eigenfunctions $g_1(\theta), g_2(\theta)$ that are optimally concentrated within a polar cap of radius $\Theta = 40^\circ$, for increasing bandwidths $L = 10, 100, 300, 600$. As the bandwidth increases, the eigenfunctions become increasingly concentrated near the pole $\theta = 0^\circ$. In any multitaper spectral application, a greater and greater fraction of any data near the boundary of the polar cap will be downweighted upon windowing; however, with increasing bandwidth and thus Shannon number, more and more well concentrated eigentapers become available, to enable the recovery of this lost information.

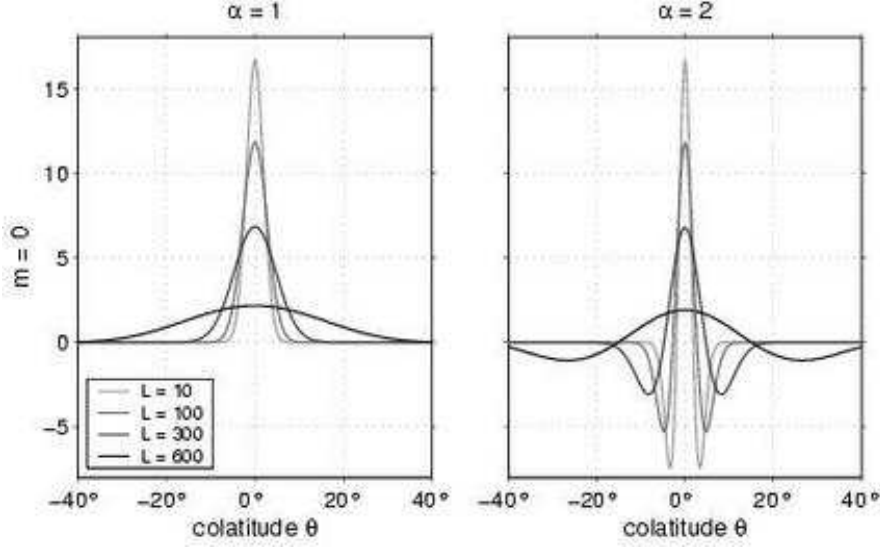


FIG. 5.8. Zonal ($m = 0$) eigenfunctions $g_1(\theta)$ (left) and $g_2(\theta)$ (right) that are optimally concentrated within an axisymmetric polar cap of colatitudinal radius $\Theta = 40^\circ$, for a range of maximal spherical harmonic degrees $L = 10, 100, 300, 600$ (increasing shades of grey). Roundoff error prevents the accurate computation of the $L = 300$ and $L = 600$ eigenfunctions by double-precision numerical diagonalization of the matrix D ; diagonalization of the Grünbaum matrix G overcomes this obstacle.

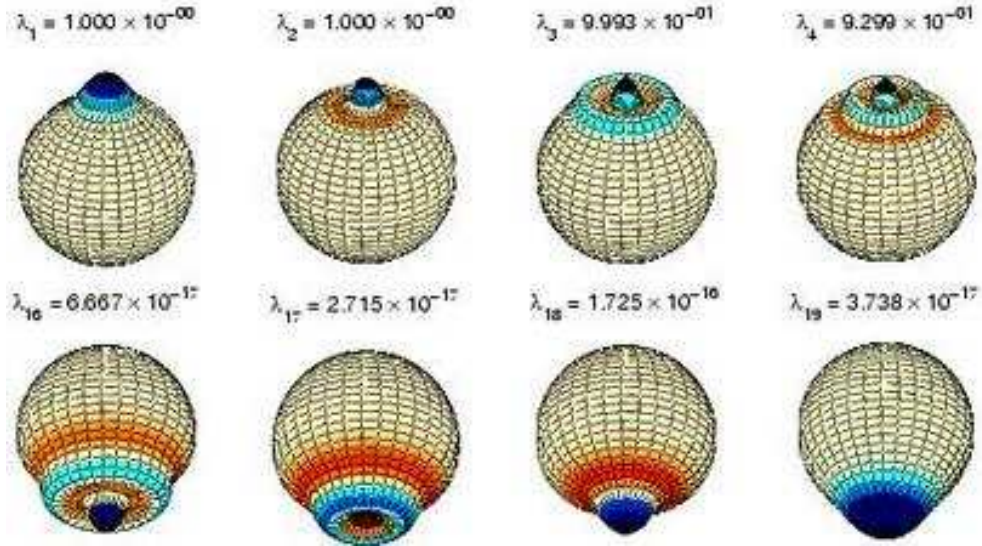


FIG. 5.9. Optimally concentrated (top row) and optimally excluded (bottom row) zonal ($m = 0$) eigenfunctions, for a circular polar cap of colatitudinal radius $\Theta = 40^\circ$ and a maximal spherical harmonic degree $L = 18$. The optimally excluded eigenfunctions cannot be accurately computed by double-precision diagonalization of the matrix D . Solution of the concentration problem for a polar cap of radius $\Theta = 140^\circ$ gives rise to the same eigenfunctions $g_1(\theta), g_2(\theta), g_3(\theta), g_4(\theta), \dots, g_{16}(\theta), g_{17}(\theta), g_{18}(\theta), g_{19}(\theta)$, but in reverse order.

Concentration within a large rather than a small polar cap is another problem for which Grünbaum's method is ideally suited. To illustrate this, we show in Figure 5.9 the first four (g_1, g_2, g_3, g_4) and the last four $(g_{16}, g_{17}, g_{18}, g_{19})$ zonal ($m = 0$) eigenfunctions, once again for a polar cap of radius $\Theta = 40^\circ$ and a maximal spherical harmonic degree $L = 18$. As noted in Section 4.3, the eigenfunctions that are optimally excluded from the polar cap $\Theta = 40^\circ$ are optimally concentrated within the much larger antipodal cap $\Theta = 140^\circ$. The actual eigenvalues $\lambda_{16}, \lambda_{17}, \lambda_{18}, \lambda_{19}$ are many orders of magnitude smaller than the listed values, which simply represent the noise floor of our double-precision computations. The optimally excluded eigenfunctions can nevertheless be accurately computed by diagonalizing the tridiagonal matrix \mathbf{G} ; this is not otherwise possible in double precision arithmetic (see Appendix A).

5.7. Abstract operator formulation. The spatial-domain commutation relation (5.25) can be expressed using the operator notation of Section 4.4 as

$$(5.45) \quad (\mathcal{R}\mathcal{H}^{-1}\mathcal{L}\mathcal{H}\mathcal{R})\mathcal{G} = \mathcal{G}(\mathcal{R}\mathcal{H}^{-1}\mathcal{L}\mathcal{H}\mathcal{R}).$$

Since the Grünbaum operator \mathcal{G} acts only upon spacelimited colatitudinal functions $h(\theta)$, it must satisfy

$$(5.46) \quad \mathcal{G} = \mathcal{G}\mathcal{R} = \mathcal{R}\mathcal{G}.$$

Upon pre-multiplying equation (5.45) by $\mathcal{L}\mathcal{H}$, post-multiplying it by $\mathcal{H}^{-1}\mathcal{L}$, and making use of the relation (5.46) and the fact that $\mathcal{L}^2 = \mathcal{L}$, we obtain

$$(5.47) \quad (\mathcal{L}\mathcal{H}\mathcal{R}\mathcal{H}^{-1}\mathcal{L})(\mathcal{L}\mathcal{H}\mathcal{G}\mathcal{H}^{-1}\mathcal{L}) = (\mathcal{L}\mathcal{H}\mathcal{G}\mathcal{H}^{-1}\mathcal{L})(\mathcal{L}\mathcal{H}\mathcal{R}\mathcal{H}^{-1}\mathcal{L}).$$

Equation (5.47) is the abstract operator formulation of the spectral-domain matrix commutation relation $\mathbf{D}\mathbf{G} = \mathbf{G}\mathbf{D}$. The operator equivalents of the spectral-domain eigenvalue equation (5.38) and the spatial-domain eigenvalue equation (5.33) are

$$(5.48a) \quad (\mathcal{L}\mathcal{H}\mathcal{G}\mathcal{H}^{-1}\mathcal{L})(\mathcal{L}\mathbf{f}) = \chi(\mathcal{L}\mathbf{f}),$$

$$(5.48b) \quad \mathcal{G}(\mathcal{R}\mathbf{f}) = \chi(\mathcal{R}\mathbf{f}),$$

where $f(\theta)$ is an arbitrary colatitudinal function, neither bandlimited nor spacelimited. Because of the commutation relations (5.45) and (5.47) we are free to solve equations (5.48) rather than the fixed-order version of equations (4.36), to find the bandlimited eigenvectors $\mathbf{g} = \mathcal{L}\mathbf{f}$ and the spacelimited eigenfunctions $h(\theta) = \mathcal{R}\mathbf{f}(\theta)$.

6. Continental Concentration. To illustrate the theory for an irregularly shaped region, we consider the spatio-spectral concentration problem in six of the Earth's continental regions, listed in Table 6.1 in order of increasing size, together with their Shannon numbers for different bandwidths. The spectral analysis of data within either the Earth's continents or oceans has a number of applications in geodesy, geophysics and oceanography [e.g., 23; 24; 45; 49]; the spherical Slepian multitapers illustrated here should be ideally suited for this task.

Figure 6.1 shows the eigenvalue spectra for five of the six regions (Greenland, Australia, North America, Africa and Eurasia) and four different bandwidths, $L = 6, 12, 18, 24$, corresponding to $(L + 1)^2 = 49, 169, 361, 625$ eigenfunctions each. The cutoff wavenumber associated with a bandwidth limit L is $\sqrt{L(L + 1)} \approx L + 1/2$ divided by the Earth's radius [5; 26]; the cutoff wavelengths corresponding to the choices $L = 6, 12, 18$ and 24 are 6200, 3200, 2200 and 1600 kilometers, respectively.

| Continental region | Area $A/(4\pi)$ in % | Shannon number N | | | |
|--------------------|----------------------|--------------------|----------|----------|----------|
| | | $L = 6$ | $L = 12$ | $L = 18$ | $L = 24$ |
| Greenland | 0.44 | 0 | 1 | 2 | 3 |
| Australia | 1.50 | 1 | 3 | 5 | 9 |
| South America | 3.50 | 2 | 6 | 13 | 22 |
| North America | 3.98 | 2 | 7 | 14 | 25 |
| Africa | 5.78 | 3 | 10 | 21 | 36 |
| Eurasia | 9.98 | 5 | 17 | 36 | 62 |

TABLE 6.1

Areas, Shannon numbers, and bandwidths for the continental concentration problem.

Only the largest of the Earth's continents, Eurasia, is sizable enough to exhibit at least one nearly perfectly concentrated eigenfunction for the smallest degree, $L = 6$, and the smallest region considered, Greenland, is too tiny to exhibit even a single eigenfunction with a concentration factor λ near unity for the largest degree, $L = 24$. As in the case of a polar cap (Figure 5.4), the rounded Shannon numbers $N = (L+1)^2 A/(4\pi)$ shown by the vertical dotted lines roughly separate the eigenfunctions with concentration factors $\lambda > 0.5$ from those with concentration factors $\lambda < 0.5$.

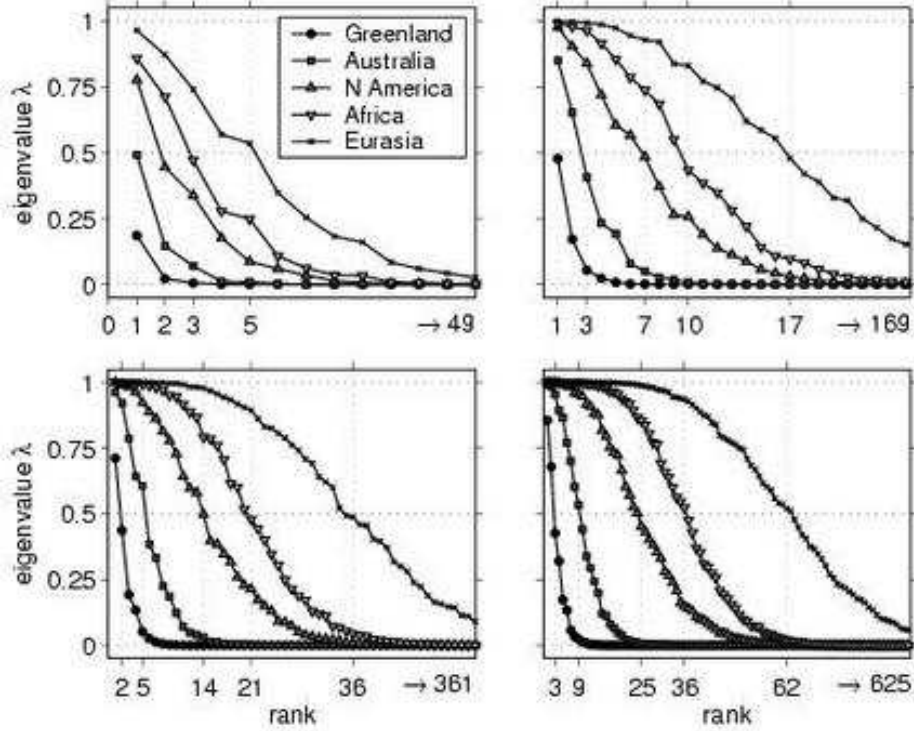


FIG. 6.1. Eigenvalue spectra for five of the Earth's continental regions (Greenland, Australia, North America, Africa, Eurasia) and four different maximal spherical harmonic degrees ($L = 6, 12, 18, 24$). Vertical gridlines and five leftmost ordinate labels specify the rounded Shannon numbers N . Ordinates are truncated on the right; number to right of arrow is the total number of eigenvalues, $(L+1)^2 = 49, 169, 361, 625$.

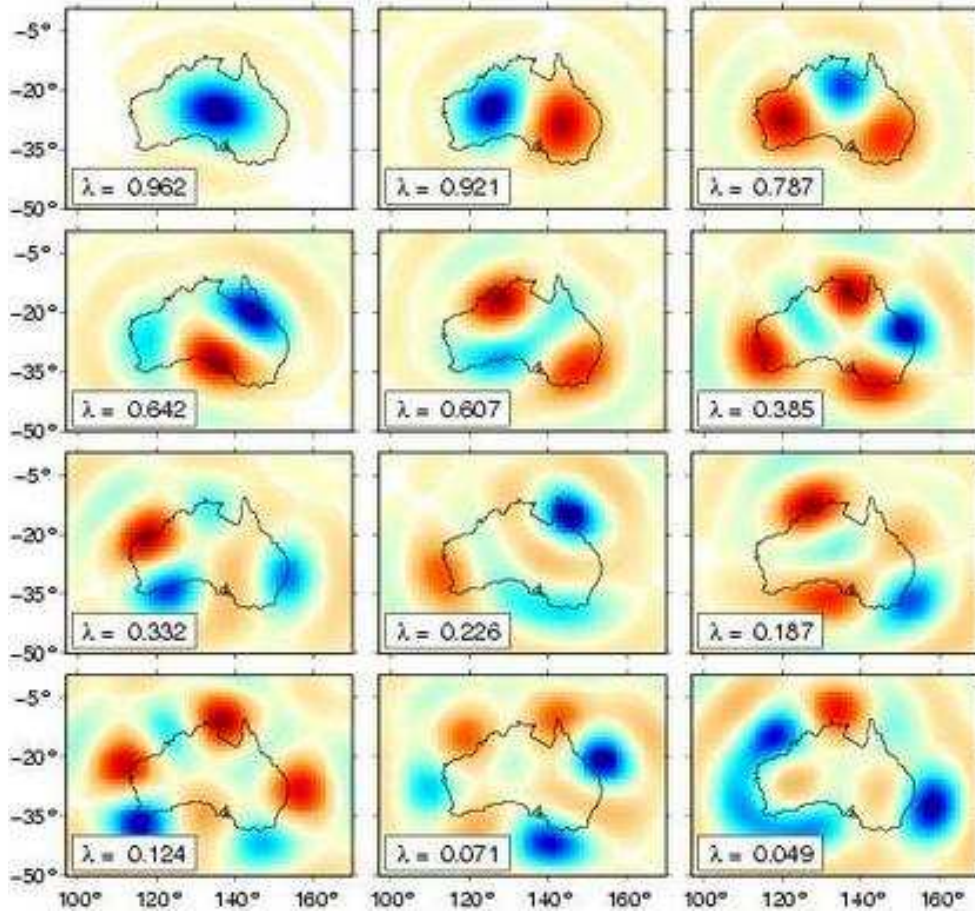


FIG. 6.2. Bandlimited $L = 18$ eigenfunctions g_1, g_2, \dots, g_{12} that are optimally concentrated within the continent of Australia. The concentration factors $\lambda_1, \lambda_2, \dots, \lambda_{12}$ are indicated; the Shannon number is $N = 5$. Order is left to right, top to bottom, as with English text.

In Figures 6.2, 6.3 and 6.4 we show map views of the first twelve $L = 18$ eigenfunctions $g_1(\hat{\mathbf{r}}), g_2(\hat{\mathbf{r}}), \dots, g_{12}(\hat{\mathbf{r}})$ that are optimally concentrated within Australia, North America and Africa. Blue colors denote positive values and red colors denote negative values (though, as we have noted, these could be reversed, since the sign of an eigenfunction is arbitrary). Regions in which the absolute value is less than one hundredth of the maximal absolute value on the sphere are rendered in white.

In the case of Australia (Figure 6.2) the first five eigenfunctions are reasonably well concentrated within the continental boundaries ($\lambda_5 = 0.607$); however, the concentration factors λ diminish rapidly thereafter, so that g_{12} is far more excluded than concentrated ($\lambda_{12} = 0.049$). With a limiting bandwidth $L = 18$, and thus a cutoff wavelength of 2200 kilometers, it is only possible to concentrate $N = 5$ orthogonal bandlimited eigenfunctions g_1, g_2, g_3, g_4, g_5 into a continent which, across its north-south waist, is only about 1500 kilometers wide.

This situation is much improved in the case of the North American continent (Figure 6.3), which has an area A that is 2.7 times larger than the area of Australia. In

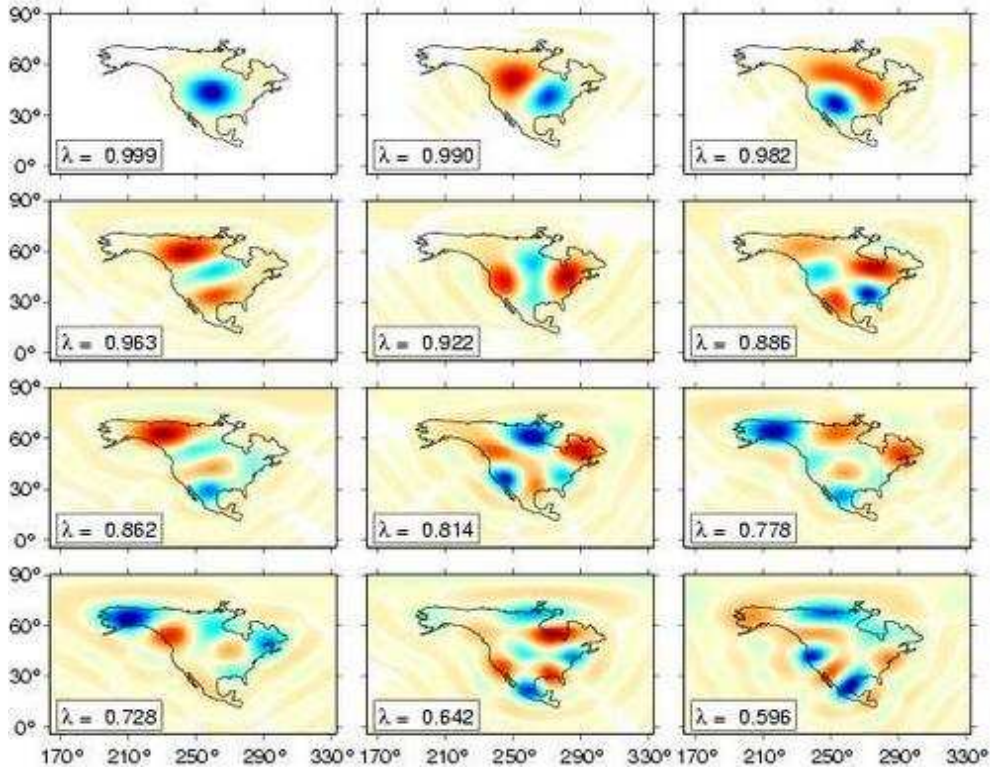


FIG. 6.3. Bandlimited $L = 18$ eigenfunctions g_1, g_2, \dots, g_{12} that are optimally concentrated within the continent of North America. The concentration factors $\lambda_1, \lambda_2, \dots, \lambda_{12}$ are indicated; the Shannon number is $N = 14$. Format is identical to that in Figure 6.2.

fact, North America has $N = 14$ reasonably well concentrated $L = 18$ eigenfunctions, of which only the first twelve are shown. The first eigenfunction, g_1 , is a roughly circular dome centered in the middle of the continent, as in the case of Australia. Subsequent orthogonal eigenfunctions g_2, g_3, \dots exhibit lobes in previously uncovered regions. The coastline of North America is more irregular than that of Australia; Québec and the Northwest Territories of Canada are essentially uncovered until g_8 , western Alaska is not adequately covered until g_9 and g_{10} , and Florida, Baja California and southern Mexico are only covered by g_{11} and g_{12} at the expense of substantial leakage ($\lambda_{11} = 0.642, \lambda_{12} = 0.596$) outside of the continental boundaries.

Africa (Figure 6.4), which has an area A that is 3.9 times larger than that of Australia, has $N = 21$ reasonably well concentrated $L = 18$ eigenfunctions, the twelfth of which has a concentration factor $\lambda_{12} = 0.887$. Once again, g_1 is roughly circular, and the subsequent orthogonal eigenfunctions g_2, g_3, \dots successively cover previously uncovered regions. West Africa is uncovered by g_1 and g_2 , but becomes reasonably well covered by g_3 and g_5 ; likewise, South Africa is uncovered until g_4 and g_5 . Other geographical features become well covered by the increasingly oscillatory orthogonal eigenfunctions (e.g., Egypt by g_7 and g_{12}).

Figure 6.5 shows the eigenvalue-weighted sum of squares $\sum_{\alpha} \lambda_{\alpha} g_{\alpha}^2(\hat{\mathbf{r}})$ of the bandlimited $L = 18$ eigenfunctions of all six of the Earth's continents (excluding Antarctica). We find the eigenfunctions $g_1(\hat{\mathbf{r}}), g_2(\hat{\mathbf{r}}), \dots, g_{(L+1)^2}(\hat{\mathbf{r}})$ by diagonalization of the

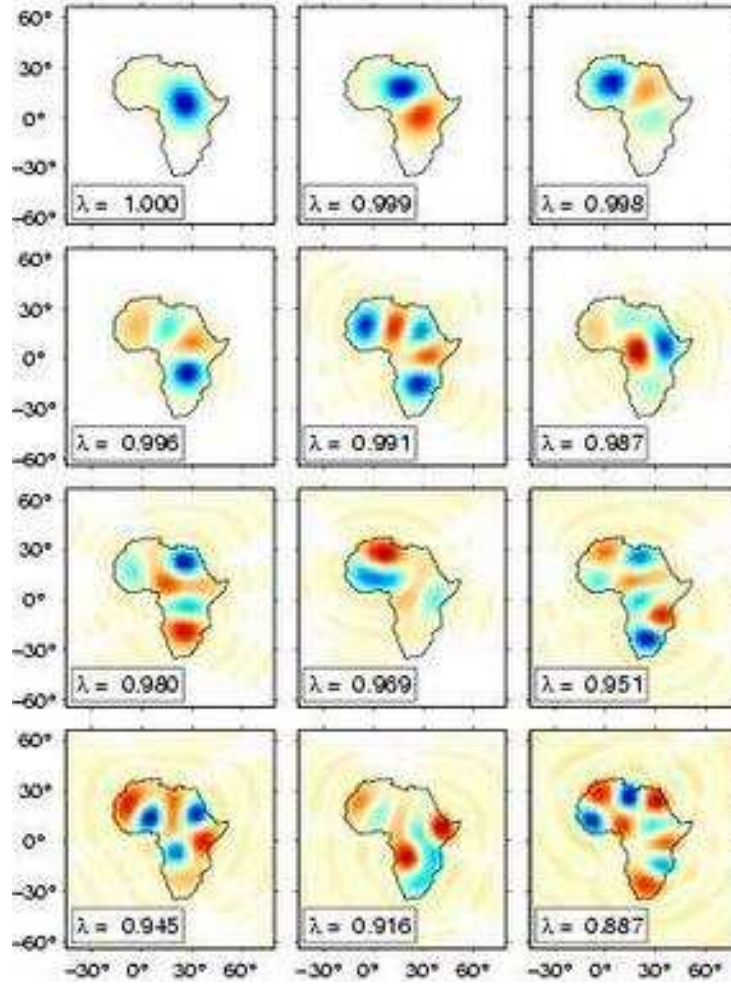


FIG. 6.4. Bandlimited $L = 18$ eigenfunctions g_1, g_2, \dots, g_{12} that are optimally concentrated within the continent of Africa. The concentration factors $\lambda_1, \lambda_2, \dots, \lambda_{12}$ are indicated; the Shannon number is $N = 21$. Format is identical to that in Figure 6.2.

$(L + 1)^2 \times (L + 1)^2$ matrix (4.5) formed by summing the corresponding matrices $\mathbf{D}_{\text{Eurasia}} + \mathbf{D}_{\text{Africa}} + \dots$ of each of the six continents. The combined area of all six continents is $A/(4\pi) = 25.2\%$, and the Shannon number is $N = 91$; the partial sums of the first $N/4$, $N/2$ and N terms, as well as the full sum of all $(L + 1)^2 = 361$ terms, are shown. The ability of the first N eigenfunctions to provide uniform coverage of the target area is evident; as in Figure 5.5, the coverage is only marginally improved by adding the remaining, poorly concentrated $(L + 1)^2 - N = 250$ terms. Due to their small size, Australia and Greenland do not appear until the $1 \rightarrow N/2$ and $1 \rightarrow N$ partial sums, respectively. Even then, the coverage of Greenland is imperfect, an expected consequence of the small Shannon number for Greenland ($N = 2$ for a maximal spherical harmonic degree $L = 18$).

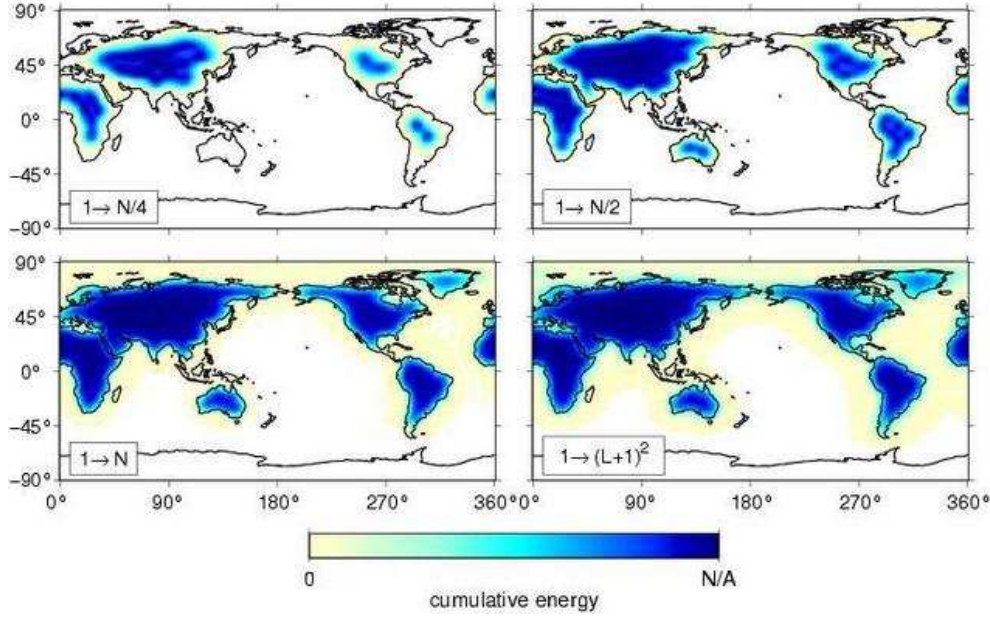


FIG. 6.5. Cumulative eigenvalue-weighted energy of the first $N/4$, $N/2$, N and all $(L+1)^2$ eigenfunctions that are optimally concentrated within the ensemble of continents Eurasia, Africa, North America, South America, Australia and Greenland. The maximal spherical harmonic degree is $L = 18$; the cumulative fractional area is $A/(4\pi) = 25.2\%$; the Shannon number is $N = 91$. Darkest blue on color bar corresponds to the expected value (4.30) of the sum, as shown. Regions in which the value is less than one hundredth of the maximal value on the sphere are rendered in white.

7. Asymptotic scaling. As we have noted, the eigenvalues $\lambda_1, \lambda_2, \dots$ and suitably scaled eigenfunctions $\psi_1(x), \psi(x)_2, \dots$ of the original Slepian concentration problem (2.6) depend only upon the Shannon number $N = 2TW/\pi$. This Shannon-number scaling is the only important feature of the one-dimensional problem that does not carry over to the spatospectral concentration problem on a sphere. Fundamentally, this lack of scaling is a consequence of the fact that it is not possible to shrink or magnify a region, such as Africa, on a sphere Ω of fixed radius $\|\hat{\mathbf{r}}\| = 1$, while keeping the angular relationships among all of the interior points the same. Shannon-number scaling on a sphere is exhibited only asymptotically, in the limit

$$(7.1) \quad A \rightarrow 0, \quad L \rightarrow \infty, \quad \text{with} \quad N = (L+1)^2 \frac{A}{4\pi} \quad \text{held fixed.}$$

In that limit of a small concentration area A and a large bandwidth $0 \leq l \leq L$, the curvature of the sphere becomes negligible and the spherical concentration problem approaches the concentration problem on a plane.

7.1. Hilb approximation and Poisson sum formula. Two results underlie the consideration of the flat-earth limit (7.1), which we undertake in this section. The first is Hilb's asymptotic approximation for the Legendre functions [2; 8; 21; 60],

$$(7.2) \quad X_{lm}(\theta) \approx (-1)^m \sqrt{\frac{l+1/2}{2\pi}} \sqrt{\frac{\theta}{\sin \theta}} J_m[(l+1/2)\theta], \quad 0 \leq \theta \ll \pi,$$

where $J_m(x)$ is the Bessel function of the first kind, and the second is the truncated Poisson sum formula,

$$(7.3) \quad \sum_{l=0}^L f(l+1/2) = \sum_{s=-\infty}^{\infty} (-1)^s \int_0^{L+1} f(k) e^{-2\pi i s k} dk,$$

which is valid for an arbitrary continuous function $f(x)$. To verify the relation (7.3) we start with the Fourier series representation of $f(x)$ on the interval $0 \leq x \leq 2\pi$,

$$(7.4) \quad f(x) = \frac{1}{2\pi} \sum_{s=-\infty}^{\infty} \int_0^{2\pi} f(u) e^{is(x-u)} du.$$

Letting $x \rightarrow x + 2\pi l$ in equation (7.4) and summing over $0 \leq l \leq L$ yields

$$(7.5) \quad \sum_{l=0}^L f(x + 2\pi l) = \frac{1}{2\pi} \sum_{s=-\infty}^{\infty} \int_0^{(L+1)2\pi} f(u) e^{is(x-u)} du,$$

where we have shifted the interval of integration for each term by $2\pi l$ and made use of the 2π periodicity of the exponential. Upon dividing the argument by 2π , substituting $k = u/(2\pi)$, and setting $x = \pi$, we obtain the desired identity (7.3).

7.2. Scaled integral equation for an arbitrary region. An application of both the Hilb approximation (7.2) and the Poisson sum formula (7.3) enables us to write the Fredholm kernel $D(\hat{\mathbf{r}}, \hat{\mathbf{r}}')$ in equation (4.15) in the form

$$(7.6) \quad \begin{aligned} D(\Delta) &= \sum_{l=0}^L \left(\frac{2l+1}{4\pi} \right) P_l(\cos \Delta) \\ &\approx \frac{1}{2\pi} \sqrt{\frac{\Delta}{\sin \Delta}} \sum_{l=0}^L (l+1/2) J_0[(l+1/2)\Delta] \\ &= \frac{1}{2\pi} \sqrt{\frac{\Delta}{\sin \Delta}} \sum_{s=-\infty}^{\infty} (-1)^s \int_0^{L+1} J_0(k\Delta) e^{-2\pi i s k} k dk. \end{aligned}$$

Upon substituting $k = (L+1)p$ and taking the limit $L \rightarrow \infty, \Delta \rightarrow 0$, with the product $L\Delta$ held fixed, equation (7.6) reduces to

$$(7.7) \quad D(\Delta) \approx \frac{(L+1)^2}{2\pi} \int_0^1 J_0[(L+1)p\Delta] p dp = \frac{(L+1) J_1[(L+1)\Delta]}{2\pi\Delta},$$

where we have made the approximation $\Delta/\sin \Delta \approx 1$, and used the Riemann-Lebesgue lemma [43] to eliminate the $s \neq 0$ terms involving the highly oscillatory factors $e^{-2\pi i s(L+1)p}$. In the limit $x \rightarrow 0$ the ratio $J_1(x)/x \rightarrow 1/2$, so the $\Delta \rightarrow 0$ limit of the kernel (7.7) is $D(0) = (L+1)^2/(4\pi)$, guaranteeing that the Shannon number, or sum of the eigenvalues (4.23), is still given in this asymptotic approximation by

$$(7.8) \quad N = \int_R D(0) d\Omega = (L+1)^2 \frac{A}{4\pi}.$$

To obtain a scaled version of equation (4.15) dependent only upon the Shannon number N , we make use of the approximation (7.7) for the kernel $D(\hat{\mathbf{r}}, \hat{\mathbf{r}}')$, and introduce the independent and dependent variable transformations

$$(7.9) \quad \mathbf{x} = \sqrt{\frac{4\pi}{A}} \hat{\mathbf{r}}, \quad \mathbf{x}' = \sqrt{\frac{4\pi}{A}} \hat{\mathbf{r}}', \quad \psi(\mathbf{x}) = g(\hat{\mathbf{r}}), \quad \psi(\mathbf{x}') = g(\hat{\mathbf{r}}').$$

The scaled coordinates \mathbf{x}, \mathbf{x}' are the projections of the points $\hat{\mathbf{r}}, \hat{\mathbf{r}}' \in \Omega$ onto a large sphere Ω_* of squared radius $\|\mathbf{x}\|^2 = 4\pi/A$. The geodesic distance between the scaled points $\mathbf{x}, \mathbf{x}' \in \Omega_*$ and the differential surface area on Ω_* are

$$(7.10) \quad \|\mathbf{x} - \mathbf{x}'\| = \sqrt{\frac{4\pi}{A}} \Delta \quad \text{and} \quad d\Omega_* = \frac{4\pi}{A} d\Omega.$$

Upon making the substitutions (7.9)–(7.10), equations (4.15) and (7.7) reduce to

$$(7.11) \quad \int_{R_*} D_*(\mathbf{x}, \mathbf{x}') \psi(\mathbf{x}) d\Omega_* = \lambda \psi(\mathbf{x}),$$

where R_* is the projection of the region of concentration R onto the sphere Ω_* , and

$$(7.12) \quad D_*(\mathbf{x}, \mathbf{x}') = \frac{\sqrt{N}}{2\pi} \frac{J_1(\sqrt{N} \|\mathbf{x} - \mathbf{x}'\|)}{\|\mathbf{x} - \mathbf{x}'\|}$$

is the symmetric, N -dependent Fredholm kernel.

Equations (7.11)–(7.12) are the spherical analogue of the one-dimensional scaled eigenvalue equation (2.6). The asymptotic eigenvalues $\lambda_1, \lambda_2, \dots$ and associated scaled eigenfunctions $\psi_1(\mathbf{x}), \psi_2(\mathbf{x}), \dots$ depend upon the maximal degree L and the area A only through the Shannon number $N = (L + 1)^2 A / (4\pi)$. As in the case of equations (4.15) and (4.19), we are free to solve (7.11)–(7.12) either on all of Ω_* , in which case the eigenfunctions $\psi_1(\mathbf{x}), \psi_2(\mathbf{x}), \dots$ are bandlimited, or only in the region of concentration R_* , in which case they are spacelimited. It is readily verified that the

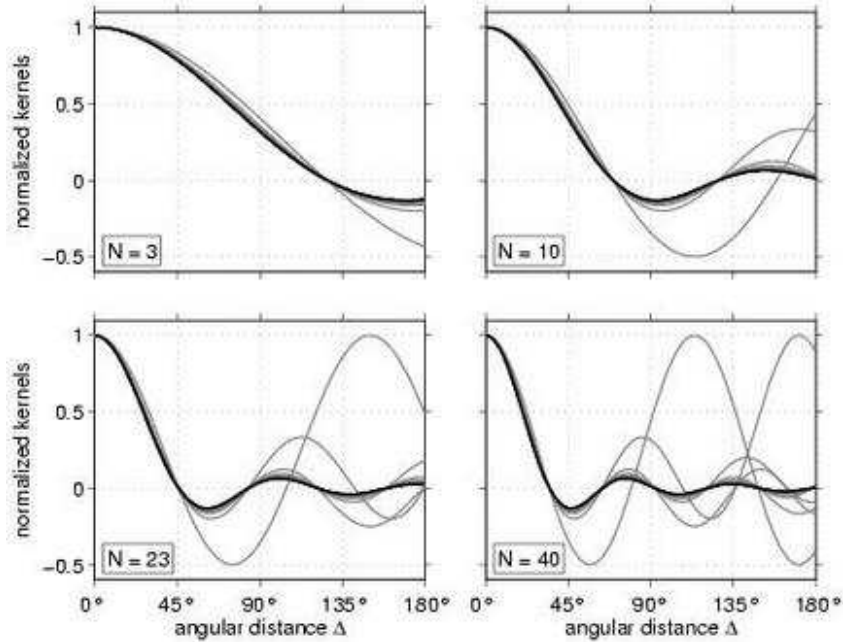


FIG. 7.1. Comparison of the exact scaled kernels (7.14) with the flat-earth asymptotic approximation (7.15) (black). The Shannon number $N = 3, 10, 23, 40$ is kept constant in each of the four panels, and the bandwidth used to compute the exact scaled kernels varies between $L = 1$ (worst fitting) and $L = 100$ (best fitting).

scaling has no effect upon the sum of the eigenvalues, inasmuch as

$$(7.13) \quad N = \int_{R_*} D_*(0) d\Omega_* = \frac{N}{4\pi} \int_{R_*} d\Omega_* = N.$$

We show in Appendix B that the scaled eigenvalue problem (7.11)–(7.12) is identical to that governing the two-dimensional concentration problem on a plane.

The above considerations show that in the limit (7.1), we expect the exact Fredholm kernel (4.14), evaluated on Ω_* and normalized by its value at zero offset,

$$(7.14) \quad \frac{D(\sqrt{4\pi/A}\Delta)}{D(0)} = \frac{1}{(L+1)^2} \sum_{l=0}^L (2l+1) P_l\left(\cos\sqrt{\frac{4\pi}{A}}\Delta\right),$$

to be well approximated by the similarly normalized asymptotic kernel

$$(7.15) \quad \frac{D_*(\Delta)}{D_*(0)} = \frac{2J_1(\sqrt{N}\Delta)}{\sqrt{N}\Delta}.$$

The quality of this asymptotic approximation to the kernel and the associated flat-earth scaling are illustrated in Figure 7.1. In the four examples shown, with Shannon numbers $N = 3, 10, 23, 40$, the approximation is excellent even for angular distances as large as $\Delta \approx 135^\circ$, once the maximal spherical harmonic degree exceeds $L = 3-4$.

7.3. Scaled eigenvalue equation for an axisymmetric polar cap. The flat-earth asymptotic version of the fixed-order colatitudinal eigenvalue problem (5.13) can be obtained in two different ways: either by an application of the Hilb approximation (7.2) and the Poisson sum formula (7.3) to the kernel $D(\theta, \theta')$ given in equation (5.14), or by using the addition theorem for Bessel functions [27],

$$(7.16) \quad J_0(k\Delta) = J_0(k\theta)J_0(k\theta') + 2 \sum_{m=1}^{\infty} J_m(k\theta)J_m(k\theta') \cos m(\phi - \phi'),$$

the representation (5.12) of $g(\theta, \phi)$, and the orthonormality of the longitudinal functions $\dots, \sqrt{2} \cos m\phi, \dots, 1, \dots, \sqrt{2} \sin m\phi, \dots$ over the interval $0 \leq \phi \leq 2\pi$ to decompose equations (4.15) and (7.7) into a series of individual eigenvalue problems, one for each order $0 \leq m \leq L$. Using either method, we find that equation (5.13) can be approximated in the limit (7.1) by

$$(7.17) \quad \int_0^\Theta D(\theta, \theta') g(\theta') \theta' d\theta' = \lambda g(\theta),$$

where

$$(7.18) \quad D(\theta, \theta') = (L+1)^2 \int_0^1 J_m[(L+1)p\theta] J_m[(L+1)p\theta'] p dp.$$

It is convenient in the present instance to approximate the area of the small polar cap by $A = 2\pi(1 - \cos \Theta) \approx \pi\Theta^2$, and to introduce scaled coordinates that are slightly different from those in equations (7.9), namely

$$(7.19) \quad x = \theta/\Theta, \quad x' = \theta'/\Theta, \quad \psi(x) = g(\theta), \quad \psi(x') = g(\theta').$$

This leads to a scaled, fixed-order eigenvalue problem,

$$(7.20) \quad \int_0^1 D_*(x, x') \psi(x') x' dx' = \lambda \psi(x),$$

with an associated kernel

$$(7.21) \quad D_*(x, x') = 4N \int_0^1 J_m(2\sqrt{N} px) J_m(2\sqrt{N} px') p dp,$$

whose eigenvalues $\lambda_1, \lambda_2, \dots$ and associated scaled eigenfunctions $\psi_1(x), \psi_2(x), \dots$ depend upon the maximal spherical harmonic degree L and the cap radius Θ only through the small polar-cap Shannon number $N = \frac{1}{4}(L+1)^2\Theta^2$.

Although the polar-cap scaling relations (7.20)–(7.21) are strictly valid only in the asymptotic limit $L \rightarrow \infty, \Theta \rightarrow 0$, the approximation is excellent even for moderate bandwidths L and sizable cap radii Θ . For a fixed Shannon number $N = 40$, a maximal degree in the range $25 \leq L \leq 40$, and therefore a cap radius $\Theta = 2\sqrt{N}/(L+1)$ in the range $29^\circ \geq \Theta \geq 18^\circ$, the agreement between the fixed-order, scaled eigenfunctions is always within a few percent. In principle, the asymptotic results (7.20)–(7.21) would enable the determination of approximate polar cap eigenfunctions $g(\theta)$ for varying values of L and Θ by scaling a pre-computed catalogue of fixed- N eigenfunctions. In practice, the construction and diagonalization of the tridiagonal Grünbaum matrix (5.44) is so straightforward and efficient that it is preferable to simply compute the optimally concentrated eigenfunctions $g(\theta)$ exactly.

7.4. Asymptotic fixed-order Shannon number. The asymptotic approximation to the number of significant eigenvalues associated with a given order m is

$$(7.22) \quad \begin{aligned} N_m &= \int_0^1 D_*(x, x) x dx \\ &= 4N \int_0^1 \int_0^1 J_m^2(2\sqrt{N} px) p dp x dx \\ &= +2N \left[J_m^2(2\sqrt{N}) + J_{m+1}^2(2\sqrt{N}) \right] \\ &\quad - (2m+1)\sqrt{N} J_m(2\sqrt{N}) J_{m+1}(2\sqrt{N}) \\ &\quad - \frac{m}{2} \left[1 - J_0^2(2\sqrt{N}) - 2 \sum_{n=1}^m J_n^2(2\sqrt{N}) \right]. \end{aligned}$$

The relationship (5.21) between the total number N of significant eigenvalues and the number N_m associated with each order m is preserved in this asymptotic approximation, inasmuch as

$$(7.23) \quad \begin{aligned} N &= N_0 + 2 \sum_{m=1}^{\infty} N_m \\ &= 4N \int_0^1 \int_0^1 \left[J_0^2(2\sqrt{N} pq) + 2 \sum_{m=1}^{\infty} J_m^2(2\sqrt{N} pq) \right] p dp x dx \\ &= 4N \int_0^1 \int_0^1 p dp x dx = N. \end{aligned}$$

In Figure 7.2 we compare the exact fixed-order Shannon numbers N_m , computed by Gauss-Legendre numerical integration of equation (5.20), with the asymptotic result (7.22), for the same values of $N = 3, 10, 23, 40$ and $1 \leq L \leq 100$ as in Figure 7.1. The number of significant $m = 0$ eigenvalues can be even more simply approximated by $N_0 \approx 2\sqrt{N}/\pi \approx (L+1)\Theta/\pi$, as shown.

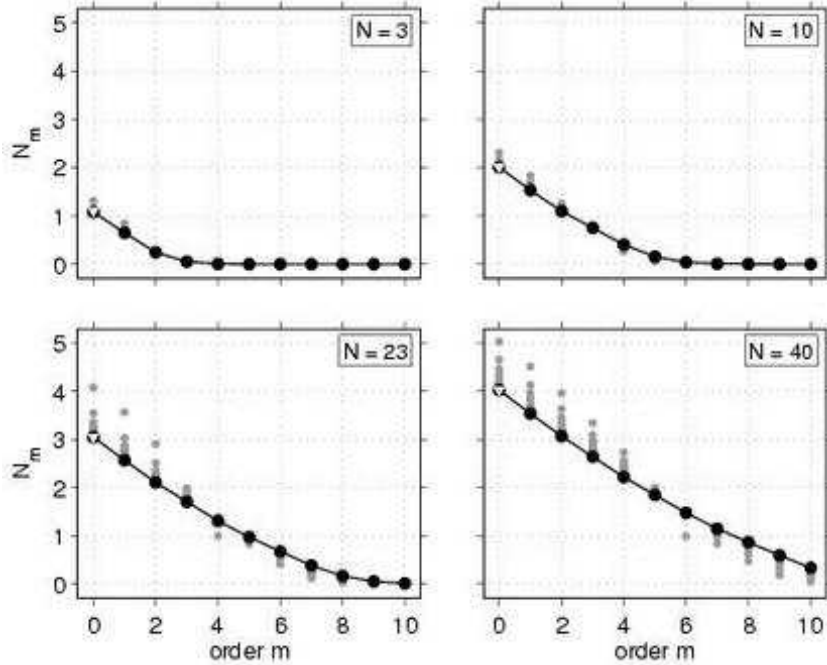


FIG. 7.2. Comparison of the number N_m of significant eigenvalues of fixed order m (grey) with the asymptotic approximation (7.22) (black). The Shannon number $N = 3, 10, 23, 40$ is kept constant in each of the four panels, and the bandwidth used to compute the exact values of N_m varies between $L = 1$ (worst fitting) and $L = 100$ (best fitting). Points inconsistent with the constraint $A/(4\pi) = N/(L+1)^2 < 1$ are not plotted. White triangles show the simplified zonal ($m = 0$) approximation $N_0 \approx (L+1)\Theta/\pi$.

8. Conclusion. An orthogonal family of bandlimited spherical harmonic expansions that are optimally concentrated within a finite region R of the unit sphere can be computed by solving either a symmetric matrix eigenvalue problem in the spectral domain or an equivalent Fredholm integral eigenvalue problem in the spatial domain. Every eigenvalue $0 < \lambda < 1$ is a measure of both the spatial concentration of the bandlimited eigenfunction $g(\hat{\mathbf{r}})$ and the spectral concentration of the spacelimited eigenfunction $h(\hat{\mathbf{r}})$ that coincides with $g(\hat{\mathbf{r}})$ inside the region of concentration. The number of well concentrated eigenfunctions is $N = (L+1)^2 A/(4\pi)$, where L is the maximal spherical degree and A is the area of the region of concentration. Roughly speaking, this Shannon number N is the dimension of the space of functions $f(\hat{\mathbf{r}})$ that can be concentrated both within a finite region R of the sphere and within a spectral interval $0 \leq l \leq L$. For a small region $A \ll 4\pi$, and a moderate maximal spherical harmonic degree L , the optimally concentrated bandlimited eigenfunctions $g(\hat{\mathbf{r}})$ and associated spacelimited eigenfunctions $h(\hat{\mathbf{r}})$ can be computed accurately, even for an irregularly shaped region R . In the special, but important, case of a circular polar

cap, every eigenfunction can be computed accurately, by numerical diagonalization of a commuting tridiagonal matrix, which has a simple Sturm-Liouville spectrum. Just as Slepian's one-dimensional, prolate spheroidal eigentapers have proven to be extremely useful in time-frequency spectral analysis, we expect the two-dimensional, spherical eigenfunctions developed here to have a wide variety of spatio-spectral data analysis applications in fields such as geophysics, planetary science and cosmology.

Acknowledgments. F. J. S. thanks Ingrid Daubechies, Peter E. Harris, Jean Steiner, Partha Mitra, Bill Symes, and David Thomson for insightful discussions, and the Département de Géophysique Spatiale et Planétaire at the Institut de Physique du Globe de Paris for their hospitality. Financial support for this work was provided by the U. S. National Science Foundation under Grant EAR-0105387. This is IPGP contribution number XXXX.

References.

- [1] A. ALBERTELLA, F. SANSÒ, AND N. SNEEUW, *Band-limited functions on a bounded spherical domain: the Slepian problem on the sphere*, J. Geodesy, 73 (1999), pp. 436–447.
- [2] R. D. AMADO, K. STRICKER-BAUER, AND D. A. SPARROW, *Semiclassical methods and the summation of the scattering partial wave series*, Phys. Rev. C, 32 (1985), pp. 329–332.
- [3] M. A. BLANCO, M. FLÓREZ, AND M. BERMEJO, *Evaluation of the rotation matrices in the basis of real spherical harmonics*, J. Mol. Struct. (Theochem), 419 (1997), pp. 19–27.
- [4] M. BÖHME AND D. POTTS, *A fast algorithm for filtering and wavelet decomposition on the sphere*, Electron. Trans. Numer. Anal., 16 (2003), pp. 70–93.
- [5] J. N. BRUNE, *Travel times, body waves, and normal modes of the Earth*, Bull. Seism. Soc. Am., 54 (1964), pp. 2099–2128.
- [6] W. E. BYERLY, *An Elementary Treatise on Fourier's Series and Spherical, Cylindrical, and Ellipsoidal Harmonics*, Ginn & Co., Boston, Mass., 1893.
- [7] R. COURANT AND D. HILBERT, *Methods of Mathematical Physics*, Interscience, New York, 1953.
- [8] F. A. DAHLEN, *A uniformly valid asymptotic representation of normal mode multiplet spectra on a laterally heterogeneous Earth*, Geophys. J. R. Astron. Soc., 62 (1980), pp. 225–247.
- [9] F. A. DAHLEN AND J. TROMP, *Theoretical Global Seismology*, Princeton Univ. Press, Princeton, N. J., 1998.
- [10] I. DAUBECHIES, *Time-frequency localization operators: A geometric phase space approach*, IEEE Trans. Inform. Theory, 34 (1988), pp. 605–612.
- [11] I. DAUBECHIES AND T. PAUL, *Time-frequency localisation operators — a geometric phase space approach: II. The use of dilations*, Inv. Probl., 4 (1988), pp. 661–680.
- [12] A. R. EDMONDS, *Angular Momentum in Quantum Mechanics*, Princeton Univ. Press, Princeton, N.J., 1996.
- [13] P. FLANDRIN, *Maximum signal energy concentration in a time-frequency domain*, in Proc. IEEE Int. Conf. Acoust. Speech Signal Process., vol. 4, IEEE, 1988, pp. 2176–2179.
- [14] P. FLANDRIN, *Time-frequency/Time-scale analysis*, Academic Press, San Diego, Calif., 1999.

- [15] W. FREEDEN AND V. MICHEL, *Orthogonal zonal, tesseral and sectorial wavelets on the sphere for the analysis of satellite data*, Adv. Comput. Math., 21 (2004), pp. 181–217.
- [16] W. FREEDEN AND M. SCHREINER, *Orthogonal and nonorthogonal multiresolution analysis, scale discrete and exact fully discrete wavelet transform on the sphere*, Constr. Approx., 14 (1998), pp. 493–515.
- [17] W. FREEDEN AND U. WINDHEUSER, *Combined spherical harmonic and wavelet expansion — A future concept in Earth’s gravitational determination*, Appl. Comput. Harm. Anal., 4 (1997), pp. 1–37.
- [18] E. N. GILBERT AND D. SLEPIAN, *Doubly orthogonal concentrated polynomials*, SIAM J. Math. Anal., 8 (1977), pp. 290–319.
- [19] F. A. GRÜNBAUM, L. LONGHI, AND M. PERLSTADT, *Differential operators commuting with finite convolution integral operators: some non-abelian examples*, SIAM J. Appl. Math., 42 (1982), pp. 941–955.
- [20] A. HANSEN, *Multidimensional multitaper spectral estimation*, Signal Process., 58 (1997), pp. 327–332.
- [21] E. HILB, *Über die Laplacesche Reihe*, Math. Z., 5 (1919), p. 17.
- [22] R. A. HORN AND C. R. JOHNSON, *Matrix Analysis*, Cambridge Univ. Press, Cambridge, UK, 1990.
- [23] C. HWANG, *Spectral analysis using orthonormal functions with a case study on sea surface topography*, Geophys. J. Int., 115 (1993), pp. 1148–1160.
- [24] C. HWANG AND S.-K. CHEN, *Fully normalized spherical cap harmonics: Application to the analysis of sea-level data from TOPEX/POSEIDON and ERS-1*, Geophys. J. Int., 129 (1997), pp. 450–460.
- [25] R. JAKOB-CHIEN AND B. K. ALPERT, *A fast spherical filter with uniform resolution*, J. Comput. Phys., 136 (1997), pp. 580–584.
- [26] J. JEANS, *The propagation of earthquake waves*, Phil. Trans. R. Soc. London, Ser. A, 102 (1923), pp. 554–574.
- [27] H. JEFFREYS AND B. S. JEFFREYS, *Methods of Mathematical Physics*, Cambridge Univ. Press, Cambridge, UK, 3 ed., 1988.
- [28] R. P. KANWAL, *Linear Integral Equations; Theory and Technique*, Academic Press, New York, 1971.
- [29] M. KIDO, D. A. YUEN, AND A. P. VINCENT, *Continuous wavelet-like filter for a spherical surface and its application to localized admittance function on Mars*, Phys. Earth Planet. Inter., 135 (2003), pp. 1–14.
- [30] H. J. LANDAU, *On the eigenvalue behavior of certain convolution equations*, Trans. Am. Math. Soc., 115 (1965), pp. 242–256.
- [31] ———, *Necessary density conditions for sampling and interpolation of certain entire functions*, Acta Mathematica Uppsala, 117 (1967), pp. 37–52.
- [32] H. J. LANDAU AND H. O. POLLAK, *Prolate spheroidal wave functions, Fourier analysis and uncertainty — II*, Bell Syst. Tech. J., 40 (1960), pp. 65–84.
- [33] ———, *Prolate spheroidal wave functions, Fourier analysis and uncertainty — III: The dimension of the space of essentially time- and band-limited signals*, Bell Syst. Tech. J., 41 (1962), pp. 1295–1336.
- [34] K. G. LIBBRECHT, *Practical considerations for the generation of large-order spherical harmonics*, Solar Physics, 99 (1985), pp. 371–373.
- [35] J. M. LILLY AND J. PARK, *Multiwavelet spectral and polarization analyses of seismic records*, Geophys. J. Int., 122 (1995), pp. 1001–1021.
- [36] T.-C. LIU AND B. D. VAN VEEN, *Multiple window based minimum variance spec-*

- trum estimation for multidimensional random fields*, IEEE Trans. Signal Process., 40 (1992), pp. 578–589.
- [37] G. MASTERS AND K. RICHARDS-DINGER, *On the efficient calculation of ordinary and generalized spherical harmonics*, Geophys. J. Int., 135 (1998), pp. 307–309.
 - [38] P. J. MCGOVERN, S. C. SOLOMON, D. E. SMITH, M. T. ZUBER, M. SIMONS, M. A. WIECZOREK, R. J. PHILLIPS, G. A. NEUMANN, O. AHARONSON, AND J. W. HEAD, *Localized gravity/topography admittance and correlation spectra on Mars: Implications for regional and global evolution*, J. Geophys. Res., 107 (2002), pp. 5136, doi:10.1029/2002JE001854.
 - [39] A. MESSIAH, *Quantum Mechanics*, Dover, New York, 2000.
 - [40] L. MIRANIAN, *Slepian functions on the sphere, generalized Gaussian quadrature rule*, Inv. Prob., 20 (2004), pp. 877–892.
 - [41] F. J. NARCOWICH AND J. D. WARD, *Nonstationary wavelets on the m-sphere for scattered data*, App. Comput. Harm. Anal., 3 (1996), pp. 324–336.
 - [42] S. OLHEDE AND A. T. WALDEN, *Generalized Morse wavelets*, IEEE Trans. Signal Process., 50 (2002), pp. 2661–2670.
 - [43] F. W. J. OLVER, *Asymptotics and Special Functions*, A. K. Peters, Wellesley, Mass., 1997.
 - [44] S. M. OULD KABER, *A Legendre pseudospectral viscosity method*, J. Comput. Phys., 128 (1996), pp. 165–180.
 - [45] R. PAIL, G. PLANK, AND W.-D. SCHUH, *Spatially restricted data distributions on the sphere: the method of orthonormalized functions and applications*, J. Geodesy, 75 (2001), pp. 44–56.
 - [46] D. B. PERCIVAL AND A. T. WALDEN, *Spectral Analysis for Physical Applications, Multitaper and Conventional Univariate Techniques*, Cambridge Univ. Press, New York, 1993.
 - [47] A. S. POLYAKOV, *Local basis expansions for linear inverse problem*, PhD thesis, New York University, 2002.
 - [48] W. H. PRESS, S. A. TEUKOLSKY, W. T. VETTERLING, AND B. P. FLANNERY, *Numerical Recipes in FORTRAN: The Art of Scientific Computing*, Cambridge Univ. Press, 2nd ed., 1992.
 - [49] S. S. SHAPIRO, B. H. HAGER, AND T. H. JORDAN, *The continental tectosphere and Earth's long-wavelength gravity field*, Lithos, 48 (1999), pp. 135–152.
 - [50] F. J. SIMONS, R. D. VAN DER HILST, AND M. T. ZUBER, *Spatio-spectral localization of isostatic coherence anisotropy in Australia and its relation to seismic anisotropy: Implications for lithospheric deformation*, J. Geophys. Res., 108 (2003), pp. 2250, doi: 10.1029/2001JB000704.
 - [51] M. SIMONS AND B. H. HAGER, *Localization of the gravity field and the signature of glacial rebound*, Nature, 390 (1997), pp. 500–504.
 - [52] M. SIMONS, S. C. SOLOMON, AND B. H. HAGER, *Localization of gravity and topography: Constraints on the tectonics and mantle dynamics of Venus*, Geophys. J. Int., 131 (1997), pp. 24–44.
 - [53] D. SLEPIAN, *Prolate spheroidal wave functions, Fourier analysis and uncertainty — IV: Extensions to many dimensions; Generalized prolate spheroidal functions*, Bell Syst. Tech. J., 43 (1964), pp. 3009–3057.
 - [54] ———, *Prolate spheroidal wave functions, Fourier analysis and uncertainty — V: The discrete case*, Bell Syst. Tech. J., 57 (1978), pp. 1371–1429.
 - [55] D. SLEPIAN, *Some comments on Fourier-analysis, uncertainty and modeling*,

- SIAM Rev., 25 (1983), pp. 379–393.
- [56] D. SLEPIAN AND H. O. POLLAK, *Prolate spheroidal wave functions, Fourier analysis and uncertainty — I*, Bell Syst. Tech. J., 40 (1960), pp. 43–63.
 - [57] D. SLEPIAN AND E. SONNENBLICK, *Eigenvalues associated with prolate spheroidal wave functions of zero order*, Bell Syst. Tech. J., 44 (1965), pp. 1745–1759.
 - [58] N. SNEEUW, *Global spherical harmonic-analysis by least-squares and numerical quadrature methods in historical perspective*, Geophys. J. Int., 118 (1994), pp. 707–716.
 - [59] SWARZTRAUBER AND W. F. SPOTZ, *Generalized discrete spherical harmonic transforms*, J. Comput. Phys., 159 (2000), pp. 213–230.
 - [60] G. SZEGÖ, *Orthogonal Polynomials*, American Mathematical Society, Providence, R.I., 4 ed., 1975.
 - [61] D. J. THOMSON, *Spectrum estimation and harmonic analysis*, Proc. IEEE, 70 (1982), pp. 1055–1096.
 - [62] F. G. TRICOMI, *Integral Equations*, Interscience, New York, 5 ed., 1970.
 - [63] D. L. TURCOTTE, R. J. WILLEMANN, W. F. HAXBY, AND J. NORBERRY, *Role of membrane stresses in the support of planetary topography*, J. Geophys. Res., 86 (1981), pp. 3951–3959.
 - [64] A. T. WALDEN, *Improved low-frequency decay estimation using the multitaper spectral-analysis method*, Geophys. Prospect., 38 (1990), pp. 61–86.
 - [65] M. A. WIECZOREK AND R. J. PHILLIPS, *Potential anomalies on a sphere: Applications to the thickness of the lunar crust*, J. Geophys. Res., 103 (1998), pp. 1715–1724.
 - [66] M. A. WIECZOREK AND F. J. SIMONS, *Localized spectral analysis on the sphere*, Geophys. J. Int., (2004), in preparation.

Appendix A. Computational considerations. Here we present a brief description of the numerical methods employed in this study. All of the computations described here have been performed using double precision arithmetic. Statements regarding machine precision refer to double precision, with a roundoff error of $\sim 10^{-16}$.

A.1. Concentration within a polar cap. We compute the colatitudinal eigenfunctions $g_1(\theta), g_2(\theta), \dots, g_{L-m+1}(\theta)$ of an axisymmetric polar cap $0 \leq \theta \leq \Theta$ using three different methods. The first method is by numerical diagonalization of the $(L - m + 1) \times (L - m + 1)$ matrix \mathbf{D} in equation (5.4). We do not implement the Wigner 3- j expression (5.7) for the matrix elements $D_{ll'}$, but instead use Gauss-Legendre quadrature [48] to evaluate the defining integral (5.6):

$$\begin{aligned}
 D_{ll'} &= \int_{\cos \Theta}^1 X_{lm}(\arccos \mu) X_{l'm}(\arccos \mu) d\mu \\
 (A.1) \quad &\approx \sum_{j=1}^J w_j X_{lm}(\arccos \mu_j) X_{l'm}(\arccos \mu_j),
 \end{aligned}$$

where $\mu_1, \mu_2, \dots, \mu_J$ are the roots of the Legendre polynomial $P_J(\bar{\mu})$, rescaled from $-1 \leq \bar{\mu}_j \leq 1$ to $\cos \Theta \leq \mu_j \leq 1$, and $w_j = 2(1 - \bar{\mu}_j^2)^{-1} [P'_J(\bar{\mu}_j)]^{-2}$, $j = 1, 2, \dots, J$ are the associated integration weights. Only the uppermost triangular matrix elements $D_{ll'}, l \leq l'$ are computed explicitly; the lowermost elements are infilled using the symmetry $D_{ll'} = D_{l'l}$. The order J of the Gauss-Legendre integration is adjusted upward until the $L - m + 1$ spatial-domain eigenfunctions $g_1(\theta), g_2(\theta), \dots, g_{L-m+1}(\theta)$

satisfy the orthogonality relations (5.11) to within machine precision. The same high-order Gauss-Legendre quadrature rule is used to evaluate the orthogonality integrals. The Legendre functions $X_{lm}(\theta)$ are computed with high accuracy to very high degree ($l \approx 500$) using a recursive algorithm [34; 37].

The second method is by numerical solution of the Fredholm equation (5.17b). Using a Gauss-Legendre quadrature rule to discretize this equation, we obtain

$$(A.2) \quad \sum_{j=1}^J w_j D(\mu_j, \mu'_j) h(\mu'_j) = \lambda h(\mu_j), \quad j = 1, 2, \dots, J.$$

Equation (A.2) can be rewritten as a symmetric algebraic eigenvalue equation,

$$(A.3) \quad (W^{1/2} \tilde{D} W^{1/2})(W^{1/2} \tilde{h}) = \lambda (W^{1/2} \tilde{h}),$$

where \tilde{h} is a J -dimensional column vector with entries $\tilde{h}_j = h(\mu_j)$, and where \tilde{D} and W denote the $J \times J$ matrices with elements $\tilde{D}_{jj'} = D(\mu_j, \mu'_{j'})$ and $W_{jj'} = w_j \delta_{jj'}$. The eigenvalues λ and transformed eigenvectors $W^{1/2} \tilde{h}$ are computed by numerical diagonalization of the matrix $W^{1/2} \tilde{D} W^{1/2}$. The order of integration J is again chosen to ensure accurate orthogonality of the spatial-domain eigenfunctions $h_1(\theta), h_2(\theta), \dots, h_{L-m+1}(\theta)$. In the zonal ($m = 0$) case the choice $J = L + 1$ renders both of the integrations (A.1) and (A.2) exact; for $m \neq 0$ we use a conservative, larger integration order J , since the integrands are no longer polynomials. The fixed-order power spectra shown in Figure 5.2 are computed by transforming the spatial-domain eigenfunctions of equation (4.19) to the spectral domain, using a spherical harmonic degree range $m \leq l \leq 127$ sufficient to avoid aliasing [58].

Even for moderate values of the maximal degree L and cap radius Θ , the smallest eigenvalues $\dots, \lambda_{L-m}, \lambda_{L-m+1}$ fall below machine precision. The associated, least well concentrated eigenfunctions computed using either of the above two direct methods are in that case essentially arbitrary orthogonal members of a numerically degenerate eigenspace, and are no longer accurate [1]. Because of this, it is not possible to find the optimally excluded eigenfunctions of a small polar cap, or equivalently the optimally concentrated eigenfunctions of a large cap, by diagonalization of either of the matrices D or \tilde{D} . Fortunately, this difficulty can be overcome by the third method, which is numerical diagonalization of the tridiagonal Grünbaum matrix (5.44). The roughly equant spacing of the Sturm-Liouville eigenvalues $\chi_1, \chi_2, \dots, \chi_{L-m+1}$ enables all of the associated eigenfunctions to be calculated to within machine precision. The spatio-spectral concentration factors $\lambda_1, \lambda_2, \dots, \lambda_{L-m+1}$ are computed to the same precision, either by *a posteriori* matrix multiplication, $\lambda = \mathbf{g}^T \mathbf{D} \mathbf{g}$, or by Gauss-Legendre integration of the equivalent spatial relation (5.11). Both the significant and the insignificant eigenvalues computed using each of the above methods agree to within machine precision, providing a useful numerical check. Diagonalization of the tridiagonal matrix \mathbf{G} is the only numerically stable way to solve the concentration problem for either a large polar cap or a large maximal degree L . By an extension of the above analysis, it is even possible to use the Grünbaum operator \mathcal{G} to compute spacelimited eigenfunctions $h_{L-m+2}(\theta), h_{L-m+3}(\theta), \dots$ that are in the null space [40].

A.2. Concentration within an arbitrarily shaped region. We solve the spatio-spectral concentration problem for an arbitrarily shaped region R by numerical diagonalization of the $(L+1)^2 \times (L+1)^2$ matrix \mathbf{D} , with elements $D_{lm, l'm'}$ defined by equation (4.4). Given the splined boundary of R , we first find the northernmost

and southernmost points, with colatitudes θ_n and θ_s . For every $\theta_n \leq \theta \leq \theta_s$, we then find the easternmost and westernmost points, with longitudes $\phi_e(\theta)$ and $\phi_w(\theta)$. In the case of a non-convex region with indentations and protuberances, there may be several such easternmost and westernmost points, which we shall index with an additional subscript $i = 1, 2, \dots, I$. The integral over longitude,

$$(A.4) \quad \Phi_{mm'}(\theta) = \sum_{i=1}^I \int_{\phi_{wi}}^{\phi_{ei}} \begin{Bmatrix} \cos m\phi \\ \sin m\phi \end{Bmatrix} \begin{Bmatrix} \cos m'\phi \\ \sin m'\phi \end{Bmatrix} d\phi,$$

can be done analytically, and we use Gauss-Legendre quadrature to compute the remaining integral over colatitude:

$$(A.5) \quad \begin{aligned} D_{lm,l'm'} &= \int_{\mu_n}^{\mu_s} X_{lm}(\arccos \mu) X_{l'm'}(\arccos \mu) \Phi_{mm'}(\arccos \mu) d\mu \\ &\approx \sum_{j=1}^J w_j X_{lm}(\arccos \mu_j) X_{l'm'}(\arccos \mu_j) \Phi_{mm'}(\arccos \mu_j). \end{aligned}$$

As in the case of a polar cap, we adjust the order of the integration J upward until the spatial-domain eigenfunctions $g_1(\hat{\mathbf{r}}), g_2(\hat{\mathbf{r}}), \dots, g_{(L+1)^2}(\hat{\mathbf{r}})$ satisfy the orthogonality relations (4.11) to within machine precision. There is no analogue of the Grünbaum operator \mathcal{G} for an arbitrarily shaped region, so only the eigenfunctions associated with eigenvalues that are above machine precision can be computed accurately. In most practical applications, this is not a limitation, since we are generally interested only in the computable, well concentrated eigenfunctions $g_1(\hat{\mathbf{r}}), g_2(\hat{\mathbf{r}}), \dots, g_N(\hat{\mathbf{r}})$, which are associated with the numerically significant eigenvalues $\lambda_1, \lambda_2, \dots, \lambda_N$.

A.3. Concentration within a non-polar circular cap. One of the principal applications of spherical Slepian functions in geophysics and planetary physics will be to analyze measurements within a circularly symmetric region centered upon an arbitrary geographical location θ_0, ϕ_0 [e.g., 29; 38; 51; 52]. The preferred procedure for determining the required optimally concentrated eigenfunctions is first to compute the spherical harmonic coefficients g_{lm} of the eigenfunctions (5.12) concentrated within a polar cap $0 \leq \theta \leq \Theta$, and then to rotate these to the desired cap location [3; 9; 12; 37]. The actual windowing of the data for further analysis may either be carried out in the spectral domain [52], or, more simply, by straightforward multiplication after transformation of the rotated eigenfunctions to the spatial domain. If one wishes to avoid spherical harmonic rotation, it is also possible to compute the rotated eigenfunctions directly, by performing the numerical integration in equation (A.4) on the analytically prescribed boundary of a cap of radius Θ centered at θ_0, ϕ_0 , given by

$$(A.6) \quad \phi_{w,e}(\theta) = \phi_0 \mp \Delta\phi(\theta) \quad \text{where} \quad \Delta\phi(\theta) = \frac{\arccos(\cos \Theta - \cos \theta \cos \theta_0)}{\sin \theta \sin \theta_0}.$$

Appendix B. Spatiospectral concentration on a plane. In one of his many papers extending the one-dimensional analysis, Slepian [53] considered the spatiospectral concentration problem in a Cartesian space of arbitrary dimension. We present a brief review of the two-dimensional Cartesian concentration problem here, for comparison with the flat-earth asymptotic analysis presented in Section 7.

An arbitrary, real-valued, square-integrable function $f(\mathbf{r})$ on the plane has the two-dimensional Fourier representation, analogous to the spherical harmonic representation (3.13),

$$(B.1) \quad f(\mathbf{r}) = \left(\frac{1}{2\pi}\right)^2 \int_{-\infty}^{\infty} F(\mathbf{k}) e^{i\mathbf{k}\cdot\mathbf{r}} d^2\mathbf{k}, \quad F(\mathbf{k}) = \int_{-\infty}^{\infty} f(\mathbf{r}) e^{-i\mathbf{k}\cdot\mathbf{r}} d^2\mathbf{r}.$$

The Fourier orthonormality relation analogous to equation (3.6) is

$$(B.2) \quad \left(\frac{1}{2\pi}\right)^2 \int_{-\infty}^{\infty} e^{i\mathbf{k}\cdot(\mathbf{r}-\mathbf{r}')} d^2\mathbf{k} = \delta(\mathbf{r}-\mathbf{r}') = \frac{\delta(\|\mathbf{r}-\mathbf{r}'\|)}{2\pi\|\mathbf{r}-\mathbf{r}'\|}.$$

Parseval's relation stipulates that the power of any function $f(\mathbf{r})$ in the spatial and spectral domains is identical:

$$(B.3) \quad \int_{-\infty}^{\infty} f^2(\mathbf{r}) d^2\mathbf{r} = \left(\frac{1}{2\pi}\right)^2 \int_{-\infty}^{\infty} |F(\mathbf{k})|^2 d^2\mathbf{k}.$$

Equation (B.3) is the planar analogue of the spherical relation $\|f\|_{\Omega}^2 = \|f\|_{\infty}^2$.

We use $g(\mathbf{r})$ to denote a bandlimited function,

$$(B.4) \quad g(\mathbf{r}) = \left(\frac{1}{2\pi}\right)^2 \int_{\|\mathbf{k}\| \leq K} G(\mathbf{k}) e^{i\mathbf{k}\cdot\mathbf{r}} d^2\mathbf{k},$$

with no power above a maximal wavenumber K . By analogy with the optimization criterion (4.2), we seek to concentrate the power of $g(\mathbf{r})$ into a finite region R :

$$(B.5) \quad \lambda = \frac{\int_R g^2 d^2\mathbf{r}}{\int_{-\infty}^{\infty} g^2 d^2\mathbf{r}} = \text{maximum}.$$

Bandlimited functions $g(\mathbf{r})$ that maximize the ratio λ in equation (B.5) are solutions to the Fourier domain eigenvalue equation, analogous to equation (4.7),

$$(B.6) \quad \int_{\|\mathbf{k}\| \leq K} D(\mathbf{k}, \mathbf{k}') G(\mathbf{k}) d^2\mathbf{k}' = \lambda G(\mathbf{k}), \quad \|\mathbf{k}\| \leq K,$$

where

$$(B.7) \quad D(\mathbf{k}, \mathbf{k}') = \left(\frac{1}{2\pi}\right)^2 \int_R e^{i(\mathbf{k}-\mathbf{k}')\cdot\mathbf{r}} d^2\mathbf{r}.$$

The corresponding problem in the spatial domain, analogous to equation (4.15), is

$$(B.8) \quad \int_R D(\mathbf{r}, \mathbf{r}') g(\mathbf{r}) d^2\mathbf{r}' = \lambda g(\mathbf{r}), \quad |\mathbf{r}| \leq \infty,$$

where

$$(B.9) \quad D(\mathbf{r}, \mathbf{r}') = \left(\frac{1}{2\pi}\right)^2 \int_{\|\mathbf{k}\| \leq K} e^{i\mathbf{k}\cdot(\mathbf{r}-\mathbf{r}')} d^2\mathbf{k}.$$

Spacelimited eigenfunctions $h(\mathbf{r})$, which vanish outside of the region R , satisfy the same eigenvalue equation (B.8), but with the domain of solution properly restricted:

$$(B.10) \quad \int_R D(\mathbf{r}, \mathbf{r}') h(\mathbf{r}) d^2 \mathbf{r}' = \lambda h(\mathbf{r}), \quad \mathbf{r} \in R.$$

The associated eigenvalue $0 < \lambda < 1$ is a measure of both the spatial concentration of $g(\mathbf{r})$ within the region R and the spectral concentration of $h(\mathbf{r})$ within the wavenumber range $\|\mathbf{k}\| \leq K$.

For consistency with (4.9), we rank order the eigenvalues so that $\lambda_1 \geq \lambda_2 \geq \dots$. The bandlimited, spatial-domain eigenfunctions $g_1(\mathbf{r}), g_2(\mathbf{r}), \dots$ may be chosen to be orthonormal over the whole plane $\|\mathbf{r}\| \leq \infty$ and orthogonal over the region R :

$$(B.11) \quad \int_{-\infty}^{\infty} g_\alpha g_\beta d^2 \mathbf{r} = \delta_{\alpha\beta} \quad \text{and} \quad \int_R g_\alpha g_\beta d^2 \mathbf{r} = \lambda_\alpha \delta_{\alpha\beta}.$$

The sum of the eigenvalues, or Shannon number, is given by

$$(B.12) \quad N = \sum_{\alpha} \lambda_\alpha = \int_{\|\mathbf{k}\| \leq K} D(\mathbf{k}, \mathbf{k}) d^2 \mathbf{k} = \int_R D(\mathbf{r}, \mathbf{r}) d^2 \mathbf{r} = K^2 \frac{A}{4\pi},$$

where A is the area of the region of concentration R . Equations (B.11) and (B.12) are the planar analogues of the spherical relations (4.11) and (4.28).

Comparison of equations (B.2) and (B.9) shows that the spatial-domain kernel $D(\mathbf{r}, \mathbf{r}')$, like its spherical counterpart $D(\hat{\mathbf{r}}, \hat{\mathbf{r}}')$, is a bandlimited delta function. Upon introducing polar coordinates and integrating over the angle, we can reduce $D(\mathbf{r}, \mathbf{r}')$ to a form reminiscent of the representation (7.7):

$$(B.13) \quad D(\mathbf{r}, \mathbf{r}') = \frac{1}{2\pi} \int_0^K J_0(k\|\mathbf{r} - \mathbf{r}'\|) k dk = \frac{K J_1(K\|\mathbf{r} - \mathbf{r}'\|)}{2\pi\|\mathbf{r} - \mathbf{r}'\|}.$$

Upon introducing scaled independent and dependent variables analogous to (7.9),

$$(B.14) \quad \mathbf{x} = \sqrt{\frac{4\pi}{A}} \mathbf{r}, \quad \mathbf{x}' = \sqrt{\frac{4\pi}{A}} \mathbf{r}', \quad \psi(\mathbf{x}) = g(\mathbf{r}), \quad \psi(\mathbf{x}') = g(\mathbf{r}'),$$

we can rewrite equations (B.8) and (B.13) in a form identical to (7.11)–(7.12) and analogous to (2.6):

$$(B.15) \quad \frac{K}{2\pi} \int_{R_*} \frac{J_1(K\|\mathbf{x} - \mathbf{x}'\|)}{\|\mathbf{x} - \mathbf{x}'\|} \psi(\mathbf{x}) = \lambda \psi(\mathbf{x}),$$

where R_* is the image of the region of concentration R under the mapping (B.14).

If the region of concentration R is a circle of radius Q , then a polar coordinate, $\mathbf{r} = (q, \phi)$, representation analogous to (5.12),

$$(B.16) \quad g(q, \phi) = \begin{cases} \sqrt{2} g(q) \cos m\phi & \text{if } -L \leq m < 0 \\ g(q) & \text{if } m = 0 \\ \sqrt{2} g(q) \sin m\phi & \text{if } 0 < m \leq L, \end{cases}$$

may be used to decompose equations (B.8) and (B.13) into a series of fixed-order eigenvalue problems analogous to (7.17)–(7.18):

$$(B.17) \quad \int_0^Q D(q, q') g(q') q' dq' = \lambda g(q),$$

where

$$(B.18) \quad D(q, q') = K^2 \int_0^1 J_m(Kpq) J_m(Kpq') p dp.$$

The transformations

$$(B.19) \quad x = q/Q, \quad x' = q'/Q, \quad \psi(x) = g(q), \quad \psi(x') = g(q')$$

convert equations (B.17)–(B.18) into the scaled eigenvalue problem

$$(B.20) \quad 4N \int_0^1 \int_0^1 J_m(2\sqrt{N}px) J_m(2\sqrt{N}px') p dp \psi(x') x' dx' = \lambda \psi(x),$$

which is identical to (7.20)–(7.21), and dependent only upon the Shannon number $N = \frac{1}{4}K^2Q^2$. Slepian [53] has noted that equation (B.20) is an iterated version of the equivalent “square root” equation

$$(B.21) \quad 2\sqrt{N} \int_0^1 J_m(2\sqrt{N}xx') \psi(x') x' dx' = \sqrt{\lambda} \psi(x).$$

The eigenvalues $\lambda_1, \lambda_2, \dots$ and eigenfunctions $\psi_1(x), \psi_2(x), \dots$ of equation (B.20) may alternatively be found by solving the equivalent equation (B.21).

In the asymptotic limit (7.1), both the general and axisymmetric spherical concentration problems are seen to be identical to the corresponding concentration problem in a plane, with the maximal wavenumber K replaced by the integer $L + 1$. The planar problem exhibits exact Shannon-number scaling analogous to that of the one-dimensional problem (2.6), whereas the scaling of the spherical problem is only asymptotic. Equation (7.22) giving the number of significant eigenvalues N_m associated with each angular order m is exact in the case of the plane.